Molecular Cell

Article

Posttranscriptional regulation of *de novo* lipogenesis by glucose-induced O-GlcNAcylation

Graphical abstract

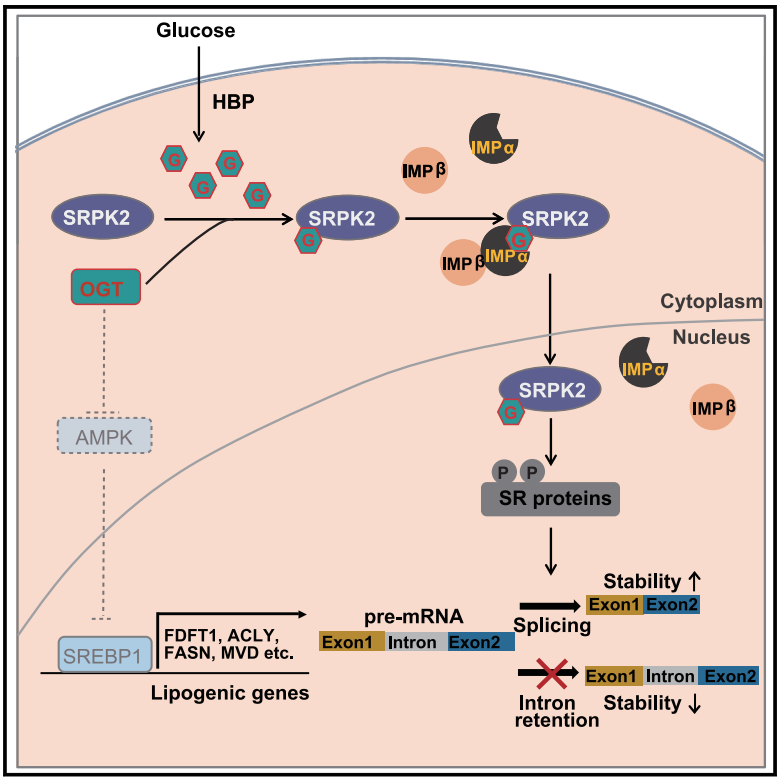

Highlights

- Interfering with O-GlcNAcylation disrupts *de novo* lipogenesis
- SRPK2 is O-GlcNAcylated at a nuclear localization signal
- Importin α proteins recognize O-GlcNAcylated nuclear localization signals
- SRPK2 O-GlcNAcylation promotes breast cancer cell growth in culture and *in vivo*

Authors

Wei Tan, Pei Jiang, Wanjun Zhang, ..., Fuchu He, Weijie Qin, Huadong Pei

Correspondence

hefc@bmi.ac.cn (F.H.),
aunp_dna@126.com (W.Q.),
huadongpei@gwu.edu (H.P.)

In brief

Lipids are necessary for cell survival and growth. Tan et al. report that SRPK2 O-GlcNAcylation at a nuclear localization signal induces its nuclear localization, promoting posttranscriptional *de novo* lipogenesis and cancer cell growth. Particularly, the O-GlcNAcylated nuclear localization signal recognized by importin α for protein nuclear import is common in cells.

Tan et al., 2021, Molecular Cell *81*, 1890–1904
May 6, 2021
https://doi.org/10.1016/j.molcel.2021.02.009

CellPress

CellPress

Molecular Cell

Article

Posttranscriptional regulation of *de novo* lipogenesis by glucose-induced O-GlcNAcylation

Wei Tan,[1,6] Pei Jiang,[2,3,6] Wanjun Zhang,[2,6] Zhaohua Hu,[3] Shaofeng Lin,[5] Lulu Chen,[3,4] Yingge Li,[3,4] Changmin Peng,[1,4] Zhuqing Li,[1,4] Aihua Sun,[2] Yali Chen,[2] Wenge Zhu,[1,4] Yu Xue,[5] Yi Yao,[3] Xiangpan Li,[3] Qibin Song,[3] Fuchu He,[2,*] Weijie Qin,[2,*] and Huadong Pei[1,4,7,*]

[1]Department of Biochemistry and Molecular Medicine, The George Washington University School of Medicine and Health Science, 2300 Eye Street, N.W., Washington, DC 20037, USA

[2]State Key Laboratory of Proteomics, National Center for Protein Sciences – Beijing, Beijing Proteome Research Center, Beijing Institute of Lifeomics, Beijing 102206, China

[3]Cancer Center, Renmin Hospital of Wuhan University, Wuhan 430062, China

[4]GW Cancer Center, George Washington University School of Medicine and Health Sciences, Washington, DC 20052, USA

[5]Key Laboratory of Molecular Biophysics of Ministry of Education, Hubei Bioinformatics and Molecular Imaging Key Laboratory, Center for Artificial Intelligence Biology, College of Life Science and Technology, Huazhong University of Science and Technology, Wuhan, Hubei 430074, China

[6]These authors contributed equally

[7]Lead contact

*Correspondence: hefc@bmi.ac.cn (F.H.), aunp_dna@126.com (W.Q.), huadongpei@gwu.edu (H.P.)

https://doi.org/10.1016/j.molcel.2021.02.009

SUMMARY

O-linked β-N-acetyl glucosamine (O-GlcNAc) is attached to proteins under glucose-replete conditions; this posttranslational modification results in molecular and physiological changes that affect cell fate. Here we show that posttranslational modification of serine/arginine-rich protein kinase 2 (SRPK2) by O-GlcNAc regulates *de novo* lipogenesis by regulating pre-mRNA splicing. We found that O-GlcNAc transferase O-GlcNAcylated SRPK2 at a nuclear localization signal (NLS), which triggers binding of SRPK2 to importin α. Consequently, O-GlcNAcylated SRPK2 was imported into the nucleus, where it phosphorylated serine/arginine-rich proteins and promoted splicing of lipogenic pre-mRNAs. We determined that protein nuclear import by O-GlcNAcylation-dependent binding of cargo protein to importin α might be a general mechanism in cells. This work reveals a role of O-GlcNAc in posttranscriptional regulation of *de novo* lipogenesis, and our findings indicate that importin α is a "reader" of an O-GlcNAcylated NLS.

INTRODUCTION

Alterations of the glucose and glutamine metabolic pathways are prevalent and physiologically important changes in cancers (Pavlova and Thompson, 2016; Altman et al., 2016; Hay, 2016; Dias and Hart, 2007). Glucose and glutamine are substrates for the hexosamine biosynthetic pathway (HBP), which generates Uridine diphosphate *N*-acetylglucosamine (UDP-GlcNAc) (Marshall et al., 1991; Hanover et al., 2010). UDP-GlcNAc is the donor for protein O-GlcNAcylation, a posttranslational modification with physiological and pathological roles (Slawson and Hart, 2011; Hanover et al., 2012; Yang et al., 2008; Reily et al., 2019). By integrated responses to nutritional stimuli, O-GlcNAcylation, which is mediated by the enzyme O-GlcNAc transferase (OGT), affects many key intracellular signaling pathways and mediates diverse cellular processes (Yang and Qian, 2017; Hardivillé and Hart, 2014). These dynamic, posttranslationally regulated signaling modules coordinate to sense and couple various environmental cues to cell fate (Hart et al., 2007, 2011). The "reader" of protein O-GlcNAcylation in cells is unknown. Generally, O-GlcNAc cycling is increased in cancers; indeed, decreasing the amount of O-GlcNAcylation can block cancer progression (de Queiroz et al., 2014; Pinho and Reis, 2015). The specific targets of O-GlcNAcylation that are important for cancer progression remain elusive.

Compared with quiescent or normal tissue, tumor cells produce more metabolic intermediates—nucleotides, amino acids, and lipids—to support essential biosynthesis and maintain rapid proliferation (DeBerardinis et al., 2008; Vander Heiden et al., 2009). Although tumor tissues can take up lipids from the microenvironment, most fatty acids for cancer cell proliferation come from *de novo* lipid synthesis (Menendez and Lupu, 2007; Baenke et al., 2013). Sterol regulatory element-binding proteins 1 and 2 (SREBP-1/2) are key transcription factors that activate expression of genes associated with *de novo* lipogenesis (Shimano and Sato, 2017; Wu and Näär, 2019). Upon cellular lipid starvation, SREBPs are activated proteolytically, leading to nuclear translocation and induction of downstream target gene

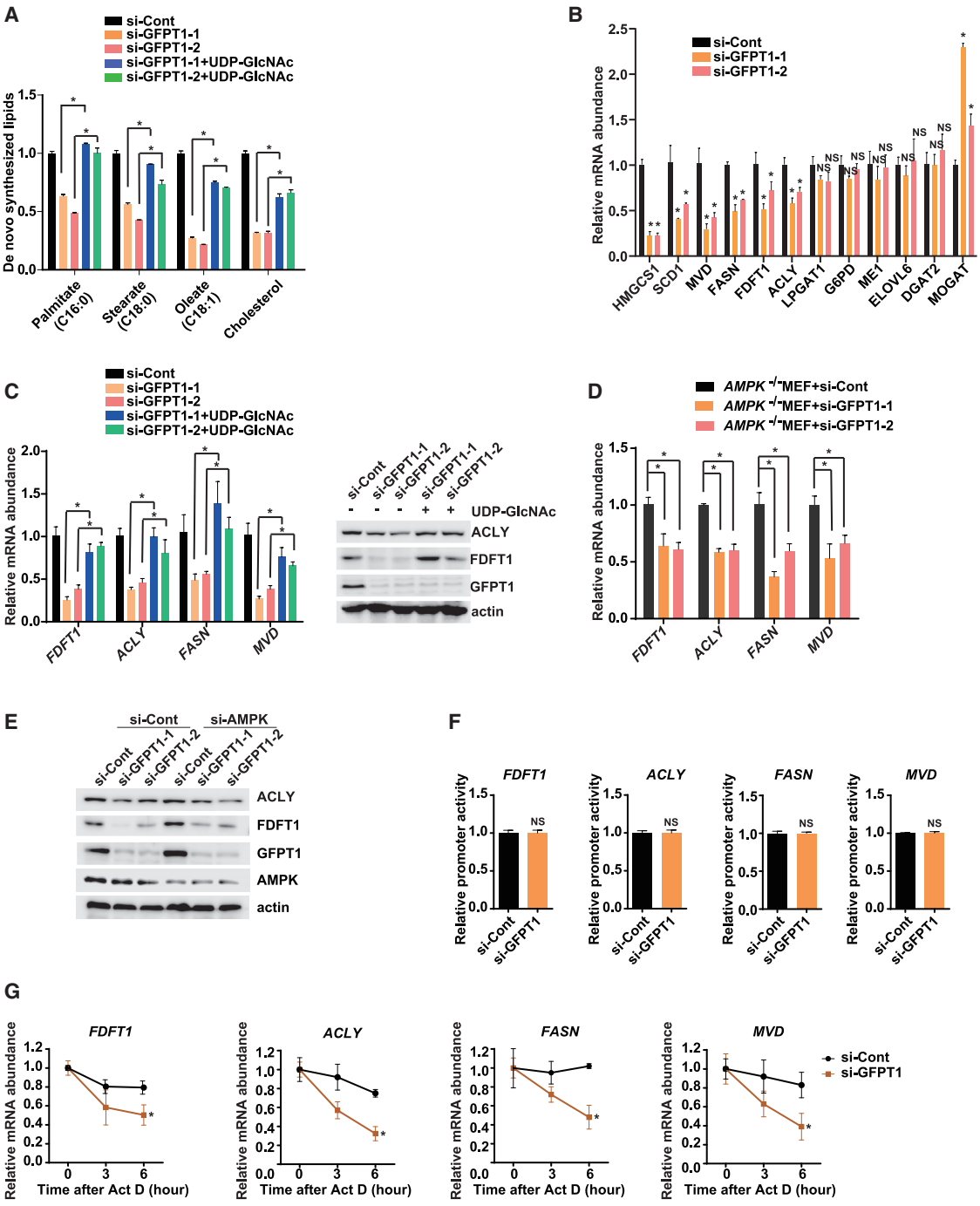

Figure 1. The HBP affects *de novo* lipogenesis at the posttranscriptional level

(A) Quantification of *de novo* lipid synthesis from U-^{13}C-glucose by liquid chromatography-mass spectrometry (LC-MS). MCF7 cells were transfected with the indicated siRNAs and deprived of serum overnight. Where indicated, 10 mM UDP-GlcNAc was added to the medium for 48 h after overnight serum starvation. Data are presented as mean ± SEM and expressed as the fold change relative to the amount in cells transfected with control siRNA (si-Cont). *$p < 0.05$ by Student's t test (n = 3, represents independent experiments throughout the text).

(B) Quantitative real-time PCR analysis of lipogenic gene mRNA in MCF7 cells. Cells transfected with siRNAs targeting GFPT1 or si-Cont were serum starved for 24 h. Data are presented as mean ± SEM and expressed as the fold change relative to the amount of transcript in cells transfected with si-Cont. *$p < 0.05$ (n = 3).

(C) Analysis of mRNA and protein for lipogenic genes in MCF7 cells. Cells were transfected with the indicated siRNAs and treated with or without 10 mM UDP-GlcNAc for 24 h after serum starvation overnight. Left: mRNA abundance was determined and expressed as the fold change relative to the amount of transcript in cells transfected with si-Cont. Data are presented as mean ± SEM. *$p < 0.05$ (n = 3). Right: ACLY and FDFT1 were detected by western blotting. Actin served as a loading control. Data are representative of 1 of 3 experiments.

(legend continued on next page)

transcription (Horton et al., 2002; Damiano et al., 2010). The gene encoding these key enzymes of *de novo* lipogenesis are frequently overexpressed in cancers, but the underlying mechanisms of their overexpression remain unclear.

In addition, *de novo* lipogenesis is tightly regulated at the post-transcriptional level. Alternative pre-mRNA splicing expands the complexity of the transcriptome and contributes to regulation of lipogenic gene expression (Vernia et al., 2016). Serine/arginine-rich protein-specific kinase 2 (SRPK2) is a key kinase that regulates pre-mRNA splicing (Wang et al., 1998; Mathew et al., 2008). Stimulation of SRPK2 in response to activation of the mechanistic target of rapamycin complex 1 (mTORC1) and ribosomal S6 kinase 1 (S6K1) pathway results in phosphorylation and activation of serine- and arginine-rich (SR) proteins, RNA-binding proteins that control splice site selection and promote pre-mRNA splicing (Lee et al., 2017). Inhibition of mTORC1 blocks SRPK2 nuclear translocation and proper function of downstream splicing factors, which induces splicing dysregulation and, thus, decreased production of the products of various lipogenic genes, including *ACLY*, *MVD*, *FDFT1*, and *FASN* (Lee et al., 2017). Therefore, SRPK2 is a potential therapeutic target to block lipogenesis and suppress growth of mTORC1-driven tumors.

Here we show that UDP-GlcNAc plays key roles in pre-mRNA splicing and *de novo* lipogenesis. Mechanistically, the OGT-SRPK2 axis promotes production of lipogenic enzymes by inducing efficient splicing of multiple mRNAs rather than affecting transcription of the encoding genes. Moreover, O-GlcNAcylation-dependent binding of cargo protein to importin α might be a general mechanism for nuclear import of protein in cells.

RESULTS

The HBP affects *de novo* lipogenesis at the posttranscriptional level

Upon exposure to hypoxia and nutrient deprivation, global protein O-GlcNAcylation in cells changes profoundly (Taylor et al., 2009; Kreppel and Hart, 1999). The HBP is a branch of glycolysis and is responsible for generating UDP-GlcNAc, the sugar donor for protein O-GlcNAcylation (Yang and Qian, 2017). Cancer cells have altered glucose metabolism and aberrant O-GlcNAcylation, suggesting altered flux through the HBP (Slawson and Hart, 2011). To investigate whether HBP regulates *de novo* lipogenesis, we knocked down glutamine-fructose-6-phosphate transaminase 1 (GFPT1), the rate-limiting enzyme in the HBP, in MCF7 cells. We measured *de novo* fatty acid synthesis in cells cultured with ^{13}C-glucose by liquid chromatography-mass spectrometry (LC-MS) (Kamphorst et al., 2013). Starving MCF7 cells of fetal bovine serum (FBS) promoted *de novo* fatty acid synthesis (Figure S1A), consistent with previous studies (Lee et al., 2017). Knockdown of GFPT1 decreased the amount of UDP-GlcNAc in cells, as expected (Figure S1B).

Under serum-free conditions, synthesis of saturated and unsaturated fatty acids and cholesterol derived from ^{13}C-glucose was reduced significantly in GFPT1-deficient MCF7 cells (Figure 1A). Addition of UDP-GlcNAc to the medium restored *de novo* lipid synthesis, indicating a role of O-GlcNAcylation (Figure 1A). Consistent with an important role of the HBP in *de novo* lipid synthesis, inhibition of HBP with small interfering RNA (siRNA) targeting GFPT1 significantly decreased the transcript abundance of multiple lipogenic genes, such as *HMGCS1*, *SCD1*, *MVD*, *FASN*, *FDFT1*, and *ACLY* (Figure 1B). We evaluated a subset of these transcripts and showed that replenishing UDP-GlcNAc in the cell culture medium restored mRNA and protein abundance (Figure 1C).

Lipogenic genes are transcriptionally induced by SREBP-1/2, which are regulated by AMP-activated protein kinase (AMPK), a cellular energy sensor (Li et al., 2011). In AMPK-deficient cells, knockdown of GFPT1 still decreased lipogenic gene mRNA and protein abundance (Figures 1D, 1E, and S1C).

A reduction in transcript abundance can result from a decrease in transcription or a decrease in mRNA stability. To evaluate the effect of GFPT1 knockdown on transcription, we analyzed the promoter activity of these genes by luciferase promoter activity assay and found no difference in promoter activity of 4 lipogenic genes in MCF7 cells in response to GFPT1 knockdown (Figure 1F). To determine whether the stability of lipogenic transcripts was affected by GFPT1 knockdown, we exposed MCF7 cells to actinomycin D to block transcription and measured the time-dependent decay of lipogenic mRNAs (Tani and Akimitsu, 2012). The stability of these transcripts was decreased markedly by GFPT1 knockdown (Figure 1G), indicating that the HBP regulates *de novo* lipogenesis at the post-transcriptional level.

OGT mediates O-GlcNAcylation, nuclear translocation, and activation of SRPK2

SRPK2 promotes lipogenic gene mRNA stability and *de novo* lipogenesis (Lee et al., 2017). Therefore, we examined whether the HBP affects *de novo* lipogenesis through SRPK2. We generated SRPK2 knockout (KO) cells using CRISPR-Cas9 technology and compared *de novo* lipogenesis in these cells with and without knockdown of OGT (Figure S1D). As expected, *de novo* lipogenesis was impaired in SRPK2 KO MCF7 cells, and this impairment was similar in these cells when OGT was also

(D) Analysis of mRNA for the indicated genes in *AMPK*$^{-/-}$ mouse embryonic fibroblasts (MEFs). Cells were transfected with the indicated siRNAs and starved of serum overnight. Transcripts were determined by quantitative real-time PCR. Data are represented as mean ± SEM. *$p < 0.05$ (n = 3).
(E) Western blot analysis of FDFT1 and ACLY in AMPK-depleted MCF7 cells. Cells were transfected with the indicated siRNAs before serum starvation overnight. Actin served as a loading control. Data are representative of 1 of 3 experiments.
(F) Promoter activity of lipogenic genes in MCF7 cells in which GFPT1 was knocked down. MCF7 cells were transfected with promoter constructs and the indicated siRNAs before serum starvation overnight. Data are represented as mean ± SEM of the fold change relative to that in si-Cont cells. *$p < 0.05$ (n = 3).
(G) Quantitative real-time PCR analysis of the stability of the lipogenic transcripts in MCF7 cells in which GFPT1 was knocked down. Data are represented as mean ± SEM. *$p < 0.05$ (n = 3).
See also Figure S1.

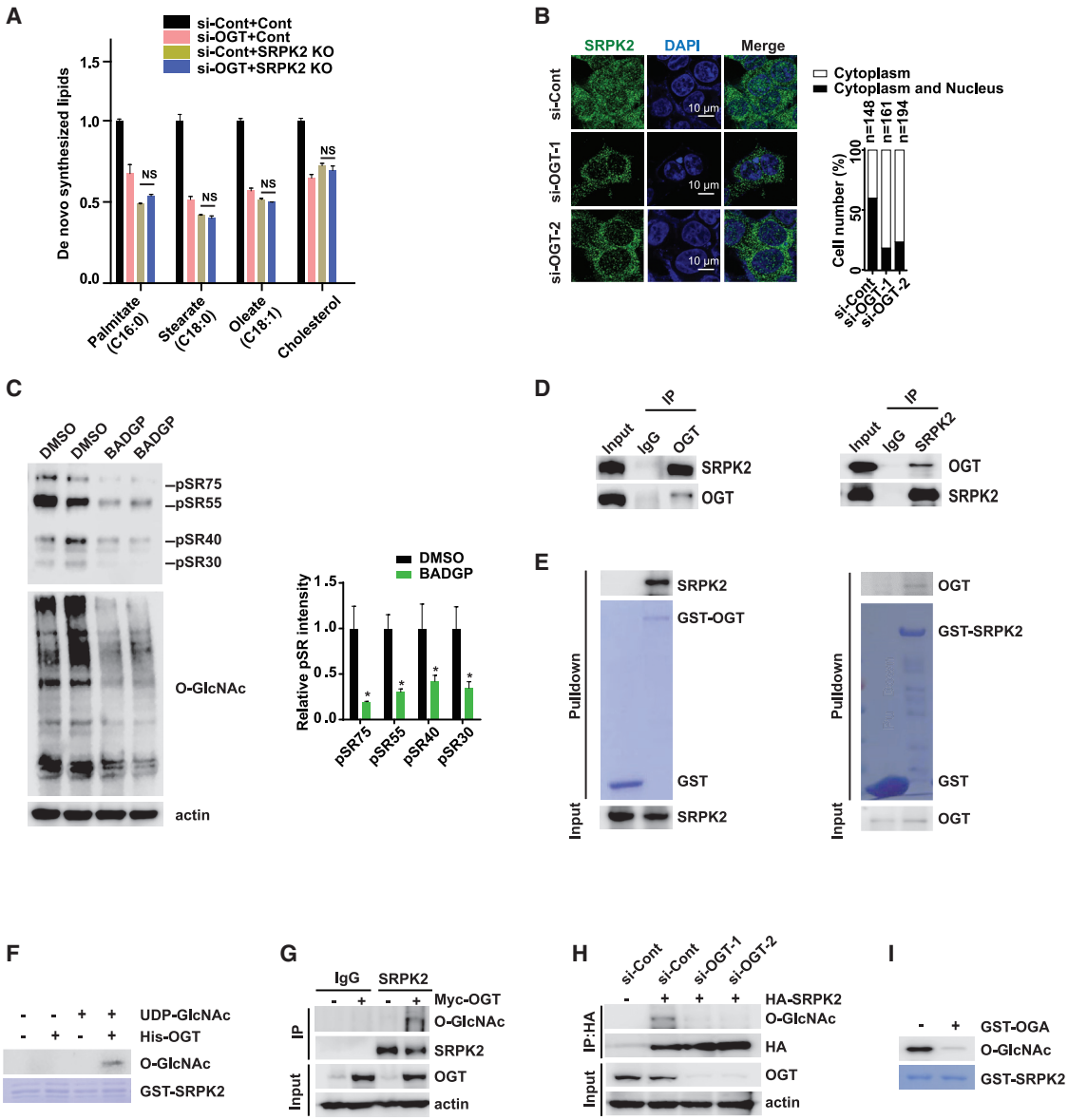

Figure 2. OGT O-GlcNAcylates SRPK2 and promotes its nuclear translocation and activation

(A) Quantification of *de novo* lipid synthesis by LC-MS. Control or SRPK2 knockout (KO) MCF7 cells were transfected with the indicated siRNAs. Cells were serum starved for 48 h. Graphs represent *de novo* synthesized lipids. Data are represented as mean ± SEM, n = 3, *p < 0.05.

(B) Immunostaining analysis of SRPK2 cellular localization in OGT-depleted cells. MCF7 cells were transfected with control or two different siRNAs targeting OGT, respectively. Left: representative images. Right: quantification of the distribution of SRPK2.

(C) MCF7 cells were treated with BADPG (5 mM) or DMSO for 48 h, and SR protein phosphorylation was examined (left). Also shown is quantification of the average band intensity of phosphorylated SR proteins normalized to β-actin (right). Data are represented as mean ± SEM; n = 2, *p < 0.05.

(D) Reciprocal endogenous immunoprecipitation (IP) was performed to detect interactions between OGT and SRPK2 in HEK293T cells.

(E) Pull-down assays were performed to detect the direct interactions between OGT and SRPK2 *in vitro*. Left: purified GST-OGT from *Escherichia coli* (*E. coli*) bacteria pulled down the purified SRPK2. Right: purified GST-SRPK2 from *E. coli* bacteria pulled down the purified OGT.

(F) *In vitro* O-GlcNAcylation assays with GST-SRPK2 (amino acids [aa] 454–521) as a substrate.

(G) HEK293T cells were transfected with the indicated plasmids. Cell lysates were immunoprecipitated with anti-SRPK2 antibody, and SRPK2 O-GlcNAcylation was determined with the indicated antibodies.

(H) HEK293T cells were transfected with the indicated siRNAs and plasmids, and SRPK2 O-GlcNAcylation was determined by IP and western blot using the indicated antibodies.

(I) O-GlcNAcylation on SRPK2 is removed by OGA *in vitro*.

See also Figure S2.

knocked down (Figure 2A). Consistent with this result, SRPK2 KO MCF7 cells exposed to the OGT inhibitor Benzyl 2-acetamido-2-deoxy-α-D-galactopyranoside (BADGP) showed no further reduction in *de novo* lipogenesis than what was observed in SRPK2 KO cells without this inhibitor (Figure S1E). BADGP effectively inhibited protein O-GlcNAcylation, as detected by western blot (Figure S1F). Similar to knocking down OGT in MCF7 cells (Figure 2A), BADGP alone also inhibited lipogenesis (Figure S1E).No greater reduction occurred when inhibition of O-GlcNAcylation by OGT knockdown or BADGP was performed with SRPK2 KO cells (Figures 2A and S1E). OGT depletion did not reduce SRPK2 abundance (Figure S1G). These data suggested that SRPK2 and OGT functioned in the same pathway to promote lipogenesis but that OGT regulated SRPK2 through mechanisms other than affecting SRPK2 abundance.

SRPK2 dynamically shuttles between the nucleus and cytoplasm and functions in the nucleus (Wang et al., 1998; Jang et al., 2009). OGT knockdown or OGT inhibitor treatment decreased nuclear and increased cytoplasmic SRPK2 staining (Figures 2B and S1H). Consistent with redistribution of SRPK2 primarily to the cytoplasm, the OGT inhibitor decreased phosphorylation of SR proteins (SR75, SR55, SR40, and SR30), which are downstream targets of SRPK2 (Figure 2C). SR protein phosphorylation by SRPK2 is required for efficient mRNA splicing of lipogenic genes (Lee et al., 2017; Kohtz et al., 1994; Cho et al., 2011). Thus, we evaluated the effect of BADGP on intron retention in mRNAs for lipogenesis proteins. We detected increased mRNA intron retention in *FDFT1*, *ACLY*, *FASN*, and *MVD* in cells exposed to the OGT inhibitor (Figure S1I).

On the basis of our findings so far, we hypothesized that SRPK2 was O-GlcNAcylated by OGT. OGT binds SRPK2 in cells and *in vitro* (Figures 2D and 2E). OGT binds SRPK2 through its C-terminal enzymatic domain, and SRPK2 binds OGT through an internal region (amino acids 257–503) (Figures S2A and S2B). Furthermore, OGT directly O-GlcNAcylated SRPK2 *in vitro* (Figure 2F). In HEK293T cells, overexpression or knockdown of OGT significantly increased or decreased SRPK2 O-GlcNAcylation, respectively (Figures 2G and 2H). N-acetyl-β-glucosaminidase (OGA) is the enzyme that removes O-GlcNAc from proteins in cells. OGA removed O-GlcNAc from SRPK2 *in vitro* (Figure 2I). Thus, OGT interacted with and O-GlcNAcylated SRPK2.

SRPK1 is a SR-specific protein kinase highly homologous to SRPK2 in cells. OGT did not interact with SRPK1 (Figure S2C), and SRPK1 was not O-GlcNAcylated in cells (Figure S2D). SRPK2 binds OGT through an internal region (Figure S2B). Interestingly, the homology of the internal regions between SRPK1 and SRPK2 is very low (Figure S2E), which explains why OGT binds SRPK2 but not SRPK1. All of these data support the hypothesis that OGT does not affect SRPK1.

OGT O-GlcNAcylates SRPK2 at Ser 490, Thr 492, and Thr 498 and promotes nuclear translocation of SRPK2

Using LC-MS/MS analysis of SRPK2 immunoprecipitated from cells, we found that threonine 237, serine 490, threonine 492, and threonine 498 were potential O-GlcNAcylation sites on SRPK2 (Figures S3A–S3D). We generated SRPK2 T237A, S490A, T492A, and T498A mutants, a mutant with S490A/T492A/T498A (3A mutant), and a 4A mutant with all four sites mutated to alanine. O-GlcNAc was reduced markedly in the SRPK2 4A mutant *in vitro* (Figure 3A). In cells, the T237A mutant appeared to be O-GlcNAcylated as much as wild-type SRPK2, whereas the other 3 individual mutants had reduced O-GlcNAcylation, and the 3A mutant had undetectable or barely detectable O-GlcNAc on western blots of the immunoprecipitated hemagglutinin (HA)-tagged protein (Figure 3B). These data indicate that S490, T492, and T498 are the main O-GlcNAcylation sites on SRPK2, but we cannot rule out the possibility of O-GlcNAcylation at other sites.

SRPK2 O-GlcNAcylation-deficient mutants (4A and 3A) exhibited decreased nuclear and increased cytoplasmic SRPK2 staining (Figure 3C). We also tested the effect of mutating the serine that is phosphorylated in response to mTORC1/S6K1 signaling, serine 494. This SRPK2 S494A mutant also exhibited a decrease in nuclear staining (Figure 3C). Reconstitution with the SRPK2 4A mutant also resulted in decreased SR protein phosphorylation for two of the evaluated SR proteins (Figures 3D and 3E). These results indicate that OGT-mediated SRPK2 O-GlcNAcylation controls cellular localization and activity of SRPK2.

SRPK2 O-GlcNAcylation at the nuclear localization signal induces its binding to importin α/β and nuclear translocation

SRPK2 contains two putative nuclear localization signals (NLSs) (Figure 4A). Deletion of the second NLS, but not the first NLS, prevented nuclear accumulation of SRPK2 in MCF7 cells (Figures 4A and 4B), suggesting that the second putative NLS is the functional one. The main O-GlcNAcylation sites of SRPK2 we identified are close to the second NLS.

Importins are proteins that mediate transport of proteins through the nuclear pore. Importins function as dimers of importin α and importin β (Miyamoto et al., 2016). There are seven importin α proteins recognizing cargo protein NLSs in cells (Goldfarb et al., 2004; Kelley et al., 2010). Importin α3, importin α5, and importin α6 appeared to contribute to nuclear localization of SRPK2 (Figures 4C and S4A). Consistent with this finding, knocking down all 3 of these importin proteins resulted in the greatest reduction in cells with nucleus-localized SRPK2 (Figure 4C). Knockdown of importin β also inhibited nuclear translocation of SRPK2 (Figures S4B and S4C).

Given these findings, we hypothesized that O-GlcNAcylation regulates nuclear translocation of SRPK2 by affecting the interaction between SRPK2 and importin α/β. Coimmunoprecipitation experiments confirmed that OGT knockdown in HEK293T cells significantly reduced binding of FLAG-tagged importin α5 with HA-tagged SRPK2 (Figure 4D) and also reduced the association of SRPK2 with importin β (Figure 4E). We evaluated importin α3, α5, and α6 in this coimmunoprecipitation assay; however, importin α3 was not expressed well, and we detected little coimmunoprecipitation between importin α6 and SRPK2 in cells expressing the control shRNA. Therefore, we could not effectively assess the effect of OGT knockdown on the interaction between SRPK2 and these two importin proteins using this experimental approach.

To evaluate the dependence of the interaction between SRPK2 and the three importins, we generated O-GlcNAcylated SRPK2 by *in vitro* O-GlcNAcylation with OGT. We compared the interaction between O-GlcNAcylated SRPK2 and unmodified

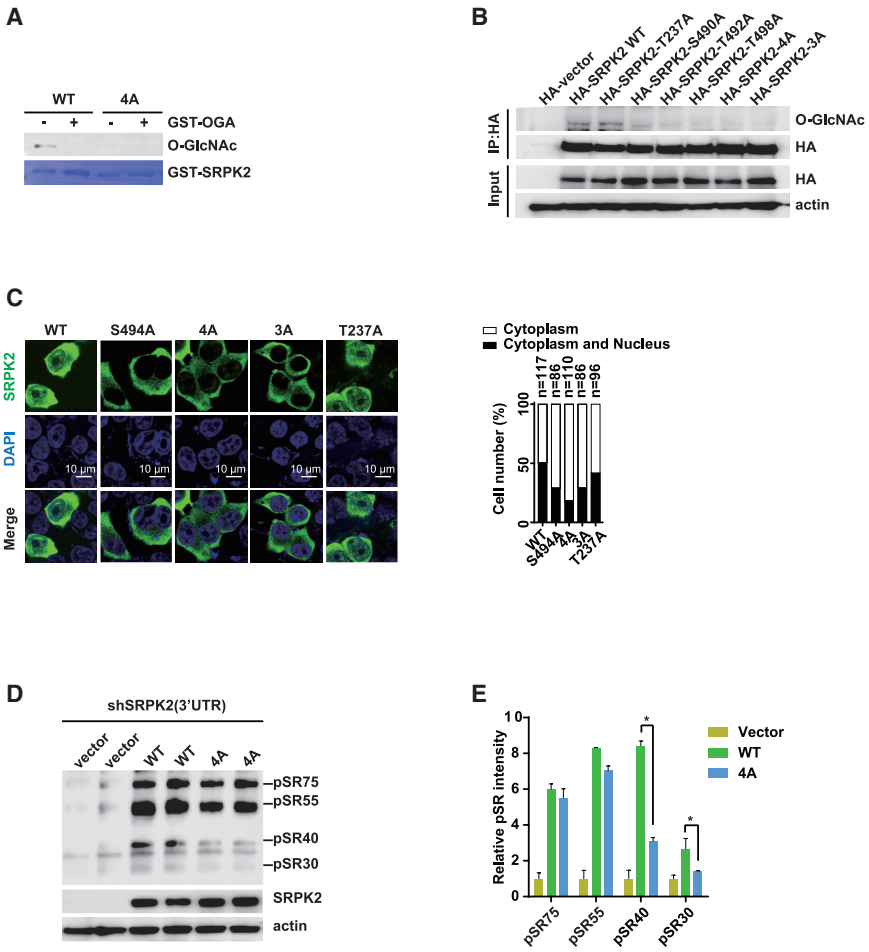

Figure 3. SRPK2 O-GlcNAcylation induces its nuclear translocation and downstream SR phosphorylation

(A) Identification of SRPK2 O-GlcNAcylation modification sites by *in vitro* O-GlcNAcylation assay. Purified GST-SRPK2 WT or 4A mutants were used as substrates.

(B) HEK293T cells were transfected with the indicated plasmids, and SRPK2 O-GlcNAcylation was analyzed by IP with an anti-HA antibody and western blots with the indicated antibodies.

(C) Endogenous SRPK2 was depleted in HEK293T cells by short hairpin RNA (shRNA) targeting the 3′ UTR of SRPK2, followed by stable reconstitution with cDNAs encoding WT or O-GlcNAcylation-deficient mutants of SRPK2 (4A or 3A or T237A). SRPK2 cellular localization was examined by immunostaining.

(D) Endogenous SRPK2 was depleted in HEK293T cells by shRNA targeting the 3′ UTR of SRPK2, followed by stable reconstitution with cDNAs encoding WT and O-GlcNAcylation-deficient mutants of SRPK2 (4A). SR protein phosphorylation was measured by western blots.

(E) Quantitative analysis of (D). Data are represented as mean ± SEM, n = 2, *p < 0.05.

See also Figure S3.

SRPK2 and importins α3, α5, and α6 using glutathione S-transferase (GST) pulldown assays. O-GlcNAcylated SRPK2 exhibited a stronger interaction than unmodified SRPK2 with the importin proteins in this *in vitro* assay, indicating that O-GlcNAcylation affects recognition of the NLS by each of these proteins (Figure 4F).

To confirm that importin α binds the O-GlcNAcylated NLS of SRPK2, we synthesized peptides corresponding to residues 487 to 523 of SRPK2. These peptides contained the second NLS and the O-GlcNAcylation sites S490, T492, and T498. We modified these peptides *in vitro* to produce O-GlcNAcylated or unmodified forms. Using surface plasmon resonance (SPR) assays, we confirmed a direct interaction between the O-GlcNAcylated peptide and importin α3 but not between the unmodified peptide and importin α3 (Figure 4G). The equilibrium dissociation constant (K_D) was calculated as 53.87 nM. These results indicate that importin α has an O-GlcNAc-dependent interaction with the NLS, suggesting that importin α is a reader of the O-GlcNAcylated NLS.

The OGT-SRPK2 pathway is parallel to the mTOR signaling pathway

SRPK2 is directly phosphorylated at Ser 494 by S6K1, a downstream target of mTORC1 (Lee et al., 2017). Ser 494 phosphorylation serves as a priming phosphorylation for subsequent phosphorylation of SRPK2 at Ser 497 by casein kinase 1 (CK1) (Lee et al., 2017). mTORC1/S6K1-dependent SRPK2 phosphorylation induces splicing of lipogenic transcripts involved in tumor growth (Lee et al., 2017). We therefore investigated whether OGT-mediated SRPK2 O-GlcNAcylation has crosstalk with mTORC1/S6K1-dependent phosphorylation. Knockdown of OGT in HEK293T cells had no effect on cellular SRPK2 Ser 494 phosphorylation (Figure 5A). Using unmodified SRPK2 or SRPK2 O-GlcNAcylated *in vitro*, we performed *in vitro* S6K1 kinase assays. O-GlcNAcylated SRPK2 and unmodified SRPK2 were substrates for S6K1-mediated phosphorylation at Ser 494 (Figure 5B). These results indicate that O-GlcNAcylation does not interfere with S6K1-mediated phosphorylation. Consistent with these *in vitro* data, inhibition of OGT in HEK293T cells with BADGP also did not reduce phosphorylation of SRPK2 at Ser 494 (Figure 5C).

As expected, exposure of HEK293T cells to an S6K1 inhibitor (PF-4708671) decreased SRPK2 Ser 494 phosphorylation (Figure 5C). S6K1 inhibition had no apparent effect on SRPK2 O-GlcNAcylation, detected by western blot of immunoprecipitated HA-tagged SRPK2 (Figure 5C). Furthermore, the SRPK2 S494A/S497A double mutant exhibited increased O-GlcNAcylation in HEK293T cells overexpressing OGT (Figure 5D).

Rapamycin is an inhibitor of mTOR. As expected, rapamycin reduced lipogenic gene transcript abundance in MCF7 cells (Figure 5E). When we knocked down OGT in rapamycin-treated cells, the abundance of the transcripts for *FDFT1*, *ACLY*, *FASN*, and *MVD* were reduced further (Figure 5E). As we observed in

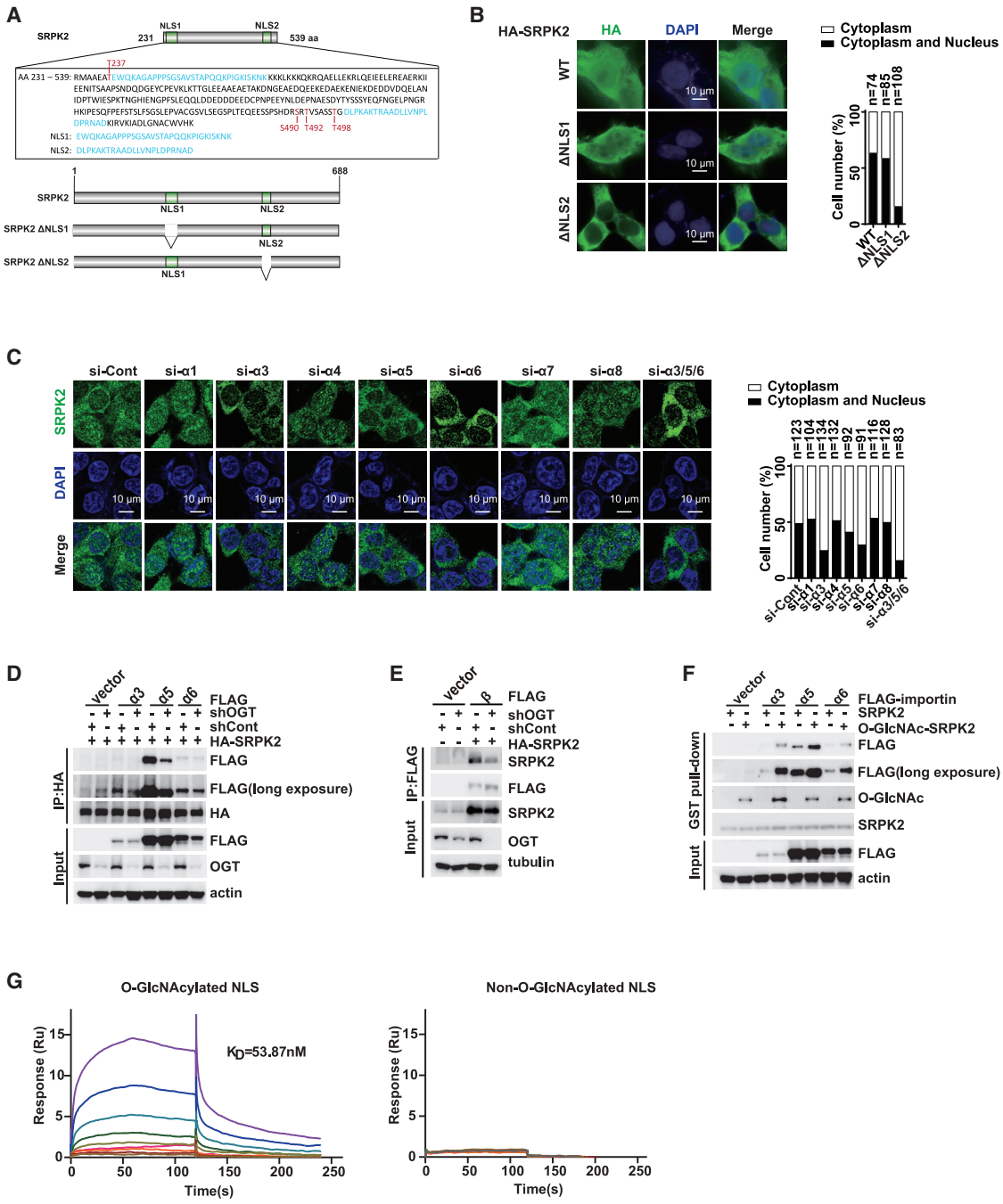

Figure 4. SRPK2 O-GlcNAcylation at NLSs induces its binding to importin α/β

(A) Amino acid sequence of the SRPK2 putative nuclear localization signals (NLSs). Locations of putative NLS1 and NLS2 are highlighted in blue, and SRPK2 O-GlcNAcylation sites are highlighted in red. The NLS was analyzed using http://nls-mapper.iab.keio.ac.jp/.

(B) Endogenous SRPK2 was depleted in MCF7 cells by shRNA targeting the 3′ UTR of SRPK2, followed by transfection with the indicated plasmids, and SRPK2 cellular localization was examined by immunostaining.

(C) MCF7 cells were transfected with the indicated siRNAs, and SRPK2 cellular localization was detected by immunostaining with an anti-SRPK2 antibody.

(D) HEK293T cells were transfected with the indicated plasmids, and the interactions between importin α3/5/6 and SRPK2 were examined by co-IP experiments.

(E) HEK293T cells were transfected with the indicated plasmids, and the interaction between importin β and SRPK2 was examined by co-IP experiments.

(F) GST-SRPK2 (aa 1–540) with O-GlcNAcylation was generated by *in vitro* glycosylation assay. HEK293T cells were transfected with the indicated importin α or vector, and cell lysates were incubated with GST-SRPK2 (aa 1–540) with or without O-GlcNAcylation.

(G) SPR characterization of the specific interactions between importin α3 and the SRPK2 NLS containing peptides with or without O-GlcNAcylation.

See also Figure S4.

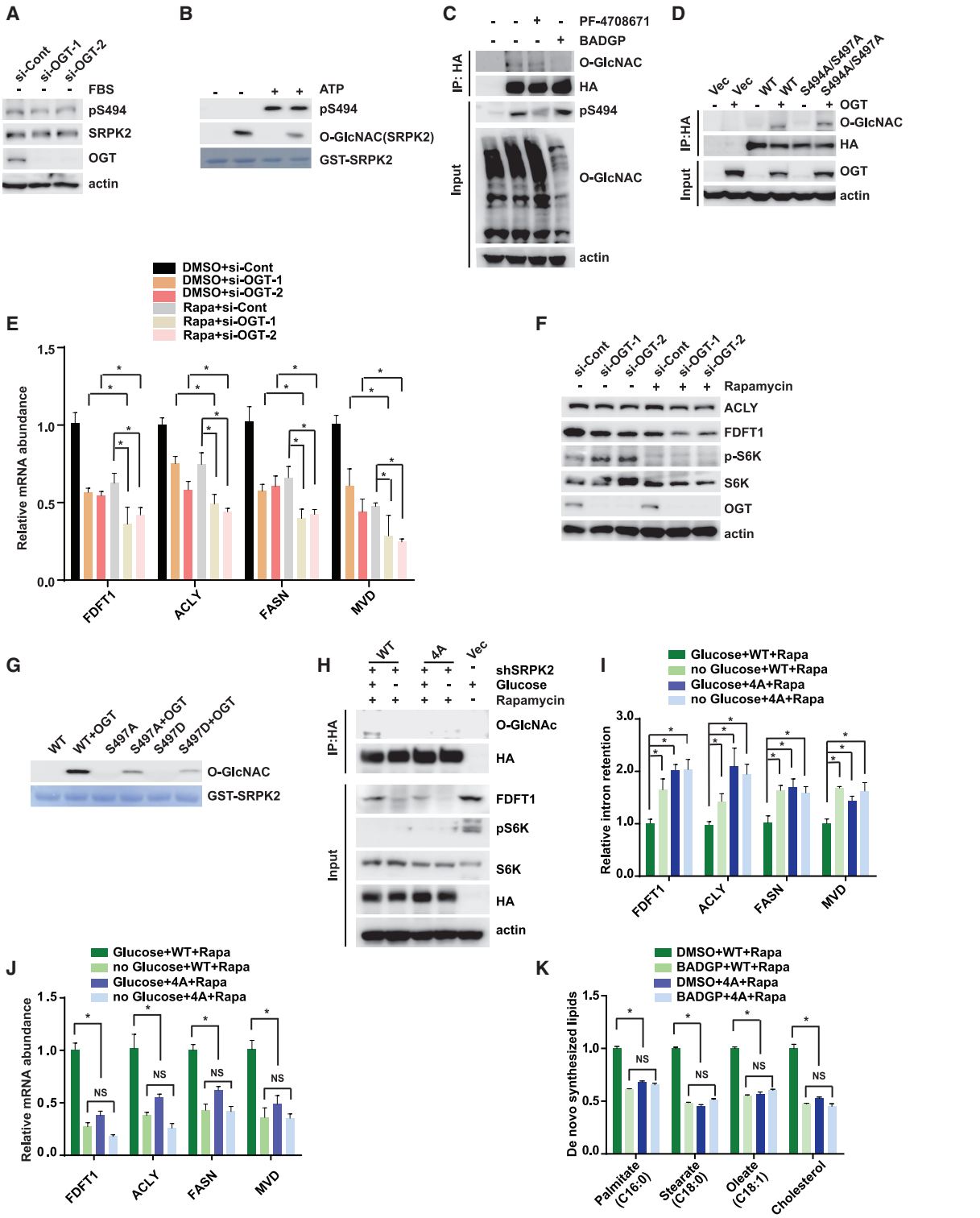

Figure 5. OGT-SRPK2 pathway is parallel to the mTOR signaling pathway

(A) HEK293T cells were transfected with the indicated siRNAs, followed by serum starvation for 24 h. SRPK2 phosphorylation was examined by western blot.

(B) *In vitro* S6K1 kinase assay with unmodified or O-GlcNAcylated SRPK2 (aa 454–521) as substrates.

(C) HEK293T cells were treated with PF-4708671 (an S6K inhibitor, 20 μM) for 24 h or BADGP (5 mM) for 48 h, and then SRPK2 O-GlcNAcylation and phosphorylation were examined by western blot.

(legend continued on next page)

response to GFPT1 knockdown (Figure 1C), the reduction in FDFT1 was greater than the reduction in ACLY at the protein level in MCF7 cells exposed to rapamycin and in which OGT was knocked down (Figure 5F). We observed a similar enhancement in the reduction of lipogenic transcripts and FDFT1 in MCF7 cells exposed to BADGP after pre-treatment with rapamycin (Figures S5A and S5B).

In the *in vitro* O-GlcNAcylation assay, the phosphorylation mimic mutant of SRPK2 (SRPK2 S497D mutant) was a substrate for OGT, although the efficiency of O-GlcNAcylation was reduced to a similar extent as observed for the SRPK2 S497A mutant (Figure 5G). These findings implied that the serine residue itself, but not its phosphorylation, affects SRPK2 O-GlcNAcylation.

To further confirm that O-GlcNAcylation regulates SRPK2 independent on mTORC1, we blocked the mTOR-dependent pathway by rapamycin, and SRPK2 O-GlcNAcylation was almost gone upon glucose starvation (Figure 5H). Glucose starvation also increased intron retention of downstream target genes (Figure 5I) and decreased their mRNA levels to levels similar to O-GlcNAcylation-deficient SRPK2 mutant (4A) cells with rapamycin treatment (Figure 5J). More importantly, BADGP (an OGT inhibitor) treatment still inhibited *de novo* fatty acid and cholesterol synthesis with rapamycin treatment (Figure 5K). OGT-mediated SRPK2 O-GlcNAcylation functions in parallel with the mTORC1/S6K1 pathway, and this is a possible glucose-sensing mechanism that needs further investigation.

SRPK2 O-GlcNAcylation promotes cellular lipid metabolism and tumorigenesis

Our results so far suggested that O-GlcNAcylation of SRPK2 promoted cellular lipid biogenesis. Using SRPK2 KO MCF7 cells, we reintroduced wild-type SRPK2, the O-GlcNAcylation-deficient SRPK2 mutants (4A or 3A), a kinase-dead mutant form of SRPK2 (K110M), or the S494A mutant, which cannot be phosphorylated by S6K1. SRPK2 KO cells had decreased synthesis of saturated and unsaturated fatty acids (Figures 6A and S6A), consistent with previous studies (Lee et al., 2017). Overexpressing wild-type SRPK2 rescued fatty acid and cholesterol synthesis but addition of the SRPK2 kinase-dead mutant (K110M) or S494A mutant (mTORC1/S6K1 phosphorylation site) did not, as expected. Additionally, neither of the SRPK2 O-GlcNAcylation-deficient mutants (4A and 3A) rescued fatty acid and cholesterol synthesis (Figure 6A), indicating that OGT-mediated SRPK2 O-GlcNAcylation promotes *de novo* lipogenesis.

We used whole-transcriptome RNA sequencing (RNA-seq) to determine whether OGT-mediated SRPK2 O-GlcNAcylation alters mRNA splicing and transcript abundance for lipid genes (Figures S6B and S6C). We detected significant differences in mRNA abundance for 1,492 genes in SRPK2 4A mutant cells compared with wild-type SRPK2 cells (Figure 6B). The differentially regulated transcripts were enriched in lipid metabolic pathways, cell death, the cell cycle, RNA splicing, and mRNA metabolic processes (Figure S6D). Transcript abundance for 42 genes among the 58 linked to lipid metabolism was decreased significantly (highlighted in green, Figure 6B). These included genes involved in *de novo* lipid synthesis, such as *ACLY*, *HMGCS1*, *FASN*, *MVD*, *FDFT1*, and *SCD* (Figures S6E–S6I). We confirmed, by quantitative real-time PCR, the reduced mRNA abundance for *FDFT1*, *ACLY*, *FASN*, and *MVD* in SRPK2 4A mutant cells (Figure 6C). We detected a changed ratio of five types of RNA splicing events in SRPK2 4A cells compared with wild-type (WT) cells, and SRPK2 4A cells showed dramatic changes in 5 types of splicing events (Figure S6J). SRPK2 4A mutant cells showed increased intron retention of these 4 lipogenic transcripts (Figures 6D and S7A–S7J).

To evaluate the pathological role of SRPK2 O-GlcNAcylation, we examined the effect of OGT-dependent SRPK2 activation in oncogenic transformation. SRPK2 knockdown in MCF7 cells reduced proliferation and colony formation, which were rescued by WT SRPK2 but not the O-GlcNAcylation-deficient mutants (Figures 6E and 6F). To test the *in vivo* relevance of these findings in the context of cancer, we conducted xenograft studies with MCF7 cells implanted in nude mice. SRPK2 knockdown significantly reduced tumor growth (Figures 6G and 6H). WT SRPK2 rescued tumor growth, but the SRPK2 4A mutant did not (Figures 6G and 6H), indicating that SRPK2 O-GlcNAcylation is important for tumor growth.

Nuclear import of proteins by O-GlcNAcylation-triggered binding of cargo protein to importin α might be a general mechanism in cells

We hypothesized that other proteins, like SRPK2, are subjected to O-GlcNAcylation near the NLS and that this enables their nuclear import. Among the dbPTM (Huang et al., 2016) and dbOGAP (Wang et al., 2011) databases and our own data, 353 proteins from humans and mice contain O-GlcNAcylation sites close to or in the NLS (Table S1). These proteins are involved in key cellular processes, such as gene transcription, protein modification, and cell death (Figure 7A). In the importin α/β

(D) HEK293T cells were transfected with the indicated plasmids, and SRPK2 O-GlcNAcylation was analyzed.
(E) MCF7 cells transfected with the indicated siRNAs were treated with or without rapamycin (100 nM) for 24 h, and then the indicated mRNA levels were examined by real-time qPCR. Data are represented as mean ± SEM; n = 3, *p < 0.05.
(F) MCF7 cells transfected with the indicated siRNAs were treated with or without rapamycin (100 nM) for 24 h, and ACLY and FDFT1 levels were examined by western blot.
(G) WT or mutant SRPK2 (S497A or S497D) proteins purified from *E. coli* were used as substrates for the *in vitro* O-GlcNAcylation assay.
(H) SRPK2-depleted MCF7 cells were transfected with the indicated plasmids and treated with rapamycin under glucose-containing or glucose-free conditions for 48 h or left untreated. SRPK2 O-GlcNAcylation, FDFT1, and pS6K1 levels were examined by western blot.
(I) Relative intron retention in (H) was determined by quantitative real-time qPCR. Data are represented as mean ± SEM; n = 3, *p < 0.05.
(J) Relative mRNA abundance in (H) was determined by quantitative real-time PCR. Data are represented as mean ± SEM; n = 3, *p < 0.05.
(K) Quantification of *de novo* lipid synthesis by LC-MS. SRPK2-depleted MCF7 cells were transfected with the indicated plasmids and treated with the indicated drugs for 48 h. Data are represented as mean ± SEM; n = 3, *p < 0.05.
See also Figure S5.

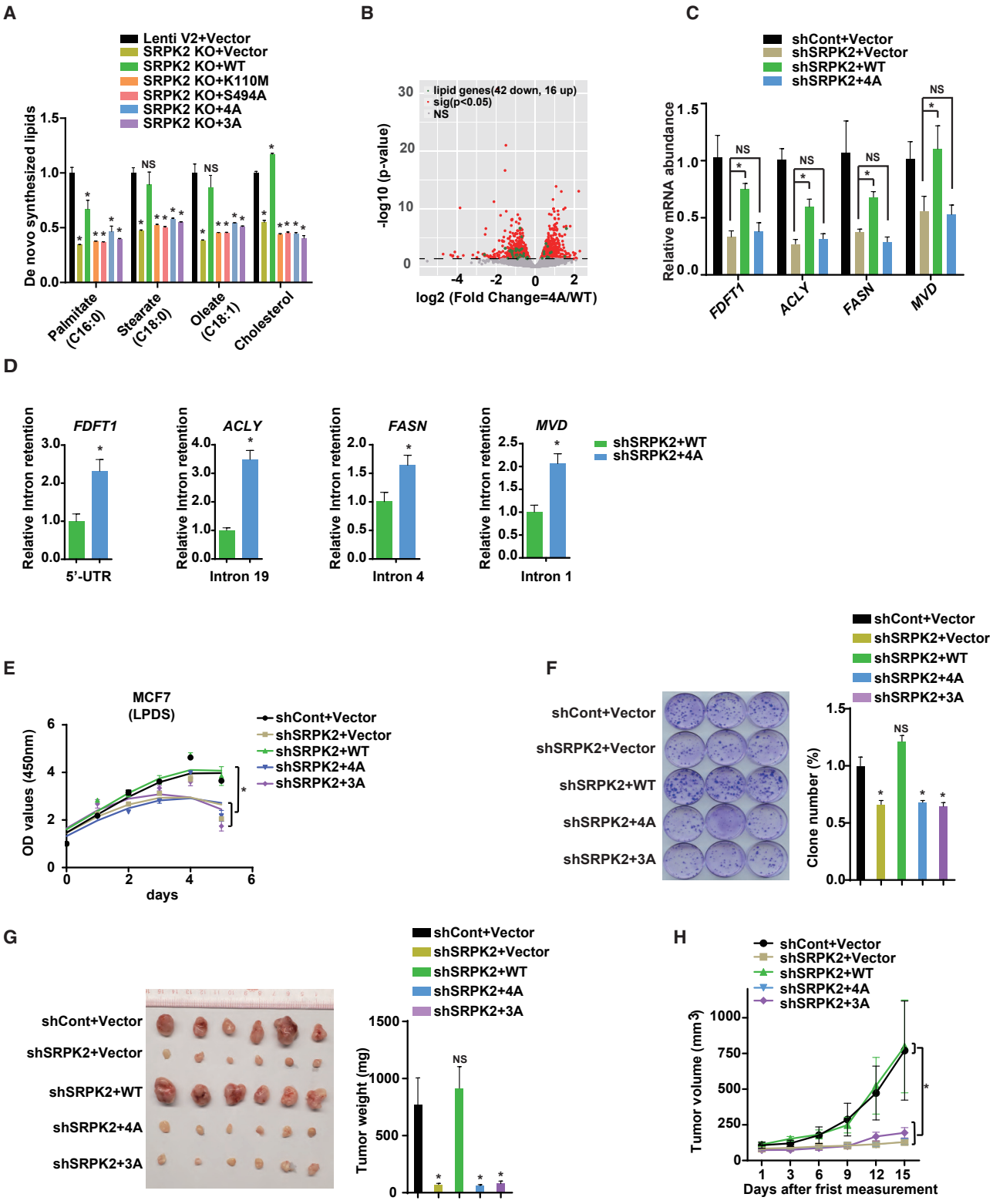

Figure 6. SRPK2 O-GlcNAcylation promotes tumorigenesis

(A) Quantification of *de novo* lipid synthesis by LC-MS. SRPK2-depleted MCF7 cells were transfected with the indicated plasmids and serum starved overnight. Data are represented as mean ± SEM; n = 3, *p < 0.05.

(legend continued on next page)

complex, importin α is an adaptor for importin β and recognizes NLS of the cargo proteins. Importin α recognizes two types of classic NLSs: a monopartite NLS with 8–10 sequential amino acids rich in lysine or arginine residues (basic residues) and a bipartite NLS with two clusters of basic residues separated by linkers of variable length and sequence (Figure 7B; Stewart, 2007; Nardozzi et al., 2010).

As a representative of proteins with a monopartite NLS, we focused on RELA (transcription factor p65), which has a conserved putative O-GlcNAcylation site at a threonine within the NLS (Figure 7B). HEK293T cells expressing HA-tagged WT RELA or the HA-tagged T305A mutant had different distributions of RELA proteins. Cells expressing T305A RELA had few cells positive for the mutant protein in the nucleus (Figure 7C), whereas a fraction of the cells expressing WT RELA were positive for nuclear WT RELA. Nuclear import of RELA depends on importin α3 (Fagerlund et al., 2005). Coimmunoprecipitation experiments with FLAG-tagged importin α3 and HA-RELA confirmed that OGT knockdown reduced the binding of importin α3 to RELA (Figure 7D). In *in vitro* GST fusion protein pulldown assays, O-GlcNAcylated RELA bound more importin α3 than unmodified RELA (Figure 7E). These results showed that O-GlcNAcylation in the NLS triggered RELA binding to importin α3 to promote nuclear import.

Other proteins have a nonclassical nuclear import signal that depends on formation of a particular tertiary structure rather than a sequence-based NLS (Nardozzi et al., 2010). To investigate whether the nuclear transport of cargo proteins with such a nuclear import signal was also regulated by O-GlcNAcylation, we studied the transcription factor Sp1. Sp1 transport into the nucleus depends on the tertiary structure formed by the 3-zinc-finger region of the C terminus (Kuwahara et al., 2000; Ito et al., 2009). There are five O-GlcNAcylation sites in this region (Chung et al., 2008; Kommaddi et al., 2011; Figure 7F). *In vitro*, OGT-mediated modification of the Sp1 5A mutant lacking the O-GlcNAcylation sites was impaired compared with O-GlcNAcylation of WT Sp1 (Figure 7G). Furthermore, expression of HA-tagged WT Sp1 or the HA-tagged Sp1 5A mutant, into HEK293T cells revealed impaired nuclear localization of the 5A mutant (Figure 7H). Consistent with previous reports that importin α3 is involved in nuclear import of Sp1 (Ito et al., 2010), we found that O-GlcNAcylation of Sp1 promoted its binding to importin α3 by coimmunoprecipitation in cells (Figure 7I) and by GST fusion protein pull-down assay (Figure 7J).

Our results supported the concept that importin α recognizes O-GlcNAcylated cargo proteins. Furthermore, by identifying 3 different proteins with different importin α recognition mechanisms, our data indicate that there may be a general mechanism for recognizing proteins destined for importin-mediated nuclear transport in cells.

DISCUSSION

Here we report an unexpected link between the HBP, a key pathway in glucose metabolism, and mTORC1/S6K1-SRPK2 in control of *de novo* lipogenesis. Our data reveal a mechanism for linking *de novo* lipogenesis to nutritional status, especially glucose availability. We found that SRPK2 is O-GlcNAcylated at an NLS by OGT. O-GlcNAcylated SRPK2 exhibited increased binding to importin α, resulting in import into the nucleus, phosphorylation of downstream SR proteins, and splicing of lipogenic pre-mRNAs. Furthermore, this axis functioned in parallel with mTOR signaling and mTOR-dependent activation of SRPK2 by phosphorylation. Thus, the OGT-SRPK2 axis is a key posttranscriptional regulator of lipid biosynthetic enzymes to support cell proliferation.

The mTORC1-S6K1 axis phosphorylates SRPK2 at Ser 494 to promote translocation from the cytoplasm to the nucleus (Lee et al., 2017). Here we found that OGT-mediated SRPK2 O-GlcNAcylation at Ser 490, Thr 492, and Thr 498 also promoted SRPK2 nuclear translocation and activation. Although SRPK2 O-GlcNAcylation sites are adjacent to the phosphorylation sites targeted by S6K1 and CK1, these two distinct posttranslational modifications did not interfere with each other on SRPK2. Inhibition of O-GlcNAcylation of SRPK2 did not affect SRPK2 phosphorylation; inhibition of the mTORC1-S6K1 pathway also did not affect SRPK2 O-GlcNAcylation.

The mTOR and HBP pathways are the major nutrient-responsive pathways that are active when cellular energy and nutrient availability are high (Dibble and Manning, 2013; Hardivillé and Hart, 2014). They are highly interconnected, but each integrates nutrient information differently. mTOR is activated by amino acids, and the HBP is triggered by ATP, uridine, glutamine, glucose, and acetyl-coenzyme A (CoA) (Bar-Peled and Sabatini, 2014; Gabriel and Kallies, 2016). Thus, coordination of the HBP and mTOR pathway enables cells to sense different environmental cues to elicit *de novo* lipogenesis.

Lipogenic enzymes are frequently mutated or upregulated in cancers (Menendez and Lupu, 2007; Currie et al., 2013), and

(B) Volcano plot analysis of the lipid genes (green) expressed differently in WT and 4A samples identified by whole-transcriptome RNA-seq in MCF7 cells. SRPK2-depleted MCF7 cells were reconstituted with WT SRPK2 or the 4A mutant, followed by serum starvation for 24 h. Genes with −log10 (adjusted p-value) > 1.30 (compared with the WT group) were considered regulated by SRPK2 O-GlcNAcylation.

(C) Endogenous SRPK2 was depleted in MCF7 cells by shRNA targeting the 3′ UTR, followed by stable reconstitution with cDNAs encoding WT or O-GlcNAcylation-deficient mutants of SRPK2. Lipogenic gene mRNA levels were analyzed by quantitative real-time PCR. Data are represented as mean ± SEM; n = 3, *p < 0.05.

(D) Intron retention analysis of the indicated genes in MCF7 cells. Cells were transfected with the indicated plasmids and serum starved for 24 h. Data are represented as mean ± SEM; n = 3, *p < 0.05.

(E) MCF7 cells were transfected with the indicated plasmids. Cells were cultured with lipoprotein-deficient serum (LPDS) for the indicated days, and cell proliferation was analyzed by cell viability assay. Data are represented as mean ± SEM; n = 3, *p < 0.05.

(F) SRPK2-depleted MCF7 cells were transfected with the indicated plasmids, and the resulting colonies were fixed and stained with crystal violet. Data are represented as mean ± SEM; n = 3, *p < 0.05.

(G and H) OGT-mediated O-GlcNAcylation of SRPK2 promotes tumor growth in xenografted mice. Tumors were weighed after mice were sacrificed at the endpoint (G). The graph represents the tumor volume after the first measurement (H). Data are represented as mean ± SEM; n = 6, *p < 0.05.

See also Figures S6 and S7.

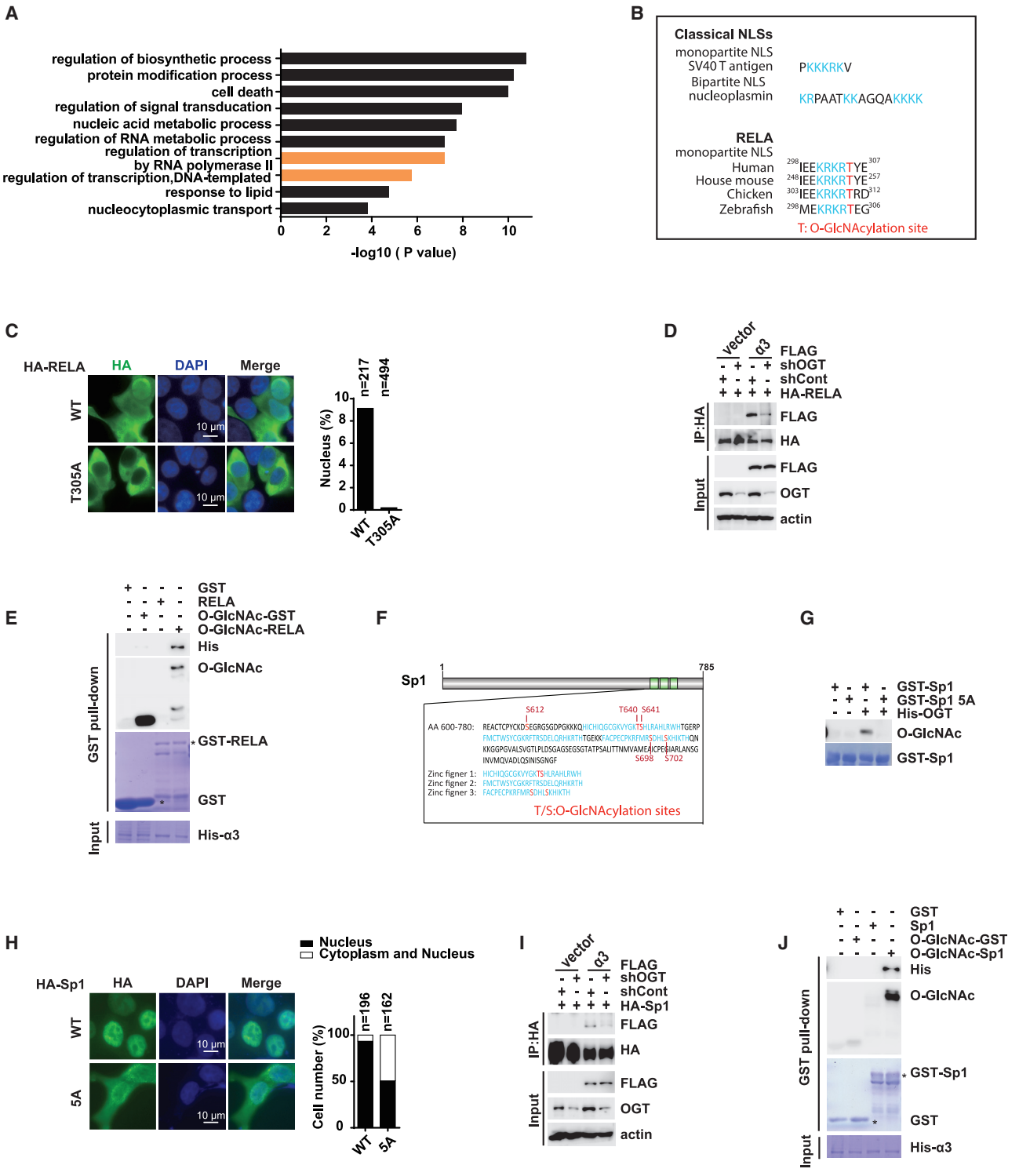

Figure 7. Nuclear import of proteins by O-GlcNAcylation-triggered binding of cargo protein to importin α might be a general mechanism in cells

(A) Gene Ontology (GO) enrichment analysis of proteins with O-GlcNAcylated NLSs from mice. The top 10 significantly ($p < 0.05$) enriched pathways are presented.

(B) Amino acid sequences of several known classic NLSs and multiple-sequence alignment of RELA across species.

(legend continued on next page)

the mTOR and SRPK2 pathways are often hyperactivated in cancers (Mossmann et al., 2018; Wang et al., 2019; Jang et al., 2008). Increased total protein O-GlcNAcylation is also common among numerous cancers, such as breast cancer (Krześlak et al., 2012; Slawson and Hart, 2011). We confirmed that OGT-mediated SRPK2 O-GlcNAcylation promoted cancer cell growth and tumorigenesis. With this axis functioning in parallel with the mTOR pathway, this suggested that dual inhibition of mTORC1/S6K1 and O-GlcNAcylation could be a promising regimen to treat cancers that depend on lipid metabolism.

We found that SRPK2 contains an importin α/β-dependent NLS (Lee et al., 2017). Importin α functions as an adaptor protein by binding the nuclear import cargo through the NLS binding domain and importin β through the Impβ binding (IBB) domain (Çağatay and Chook, 2018). Importin β docks the ternary import complex at the nuclear pore complex and promotes its translocation through the nuclear pore complex into the nucleus (Macara, 2001). Our *in vitro* and cellular data indicate that OGT-mediated SRPK2 O-GlcNAcylation promotes SRPK2 binding to importin α3, α5, and α6 and suggest that importin α is a reader of O-GlcNAcylated NLSs. O-GlcNAcylation modification may induce changes in NLS conformation, triggering NLS binding to importin α3, α5, or α6 and nuclear import of SRPK2.

Based on bioinformatics analysis, we identified 353 proteins with putative O-GlcNAcylation events close to or in their NLSs. O-GlcNAcylation promotes interactions between RELA or Sp1 and importin proteins and enhances their nuclear localization. Our findings support a model where O-GlcNAcylation-dependent binding of cargo proteins to importin α might be a general mechanism for nuclear transport in response to changes in glucose availability. The molecular details of how O-GlcNAc influences the interaction between cargo and the importin α/β complex await 3D structure analyses of the importin α/β complex with cargoes with non-O-GlcNAcylated or O-GlcNAcylated NLSs. O-GlcNAcylation-dependent regulation of NLS function may enable cells to properly regulate protein nuclear localization in response to changes in nutrient status.

STAR★METHODS

Detailed methods are provided in the online version of this paper and include the following:

SUPPLEMENTAL INFORMATION

Supplemental information can be found online at https://doi.org/10.1016/j.molcel.2021.02.009.

ACKNOWLEDGMENTS

We thank John Blenis (Weill Cornell Medicine, Sandra and Edward Meyer Cancer Center) for his gift of the HA-SRPK2 plasmid. H.P. was supported by research scholar grant RSG-19-032-01-DMC from the American Cancer Society and the Pediatric Brain Tumor Grant Award from the Childhood Brain Tumor Foundation.

(C) HEK293T cells were transfected with the indicated plasmids, and RELA cellular localization was examined by immunostaining. Left: representative images. Right: statistical analysis of the left panel.
(D) HEK293T cells were transfected with indicated shRNAs and plasmids, and the interactions between importin α3 and RELA were examined by co-IP experiments.
(E) His-importin α was purified from *E. coli* BL21. His-importin α was incubated with beads binding GST-RELA (aa 200–350) with or without O-GlcNAcylation.
(F) Amino acid sequence of the Sp1 3-zinc-finger domain.
(G) *In vitro* O-GlcNAcylation assays with GST-Sp1 (aa 600–780) or GST-Sp1 (aa 600–780) 5A as a substrate.
(H) HEK293T cells were transfected with the indicated plasmids, and Sp1 cellular localization was examined by immunostaining. Left: representative images. Right: statistical analysis of the left panel.
(I) HEK293T cells were transfected with the indicated shRNAs and plasmids, and the interactions between importin α3 and Sp1 were examined by co-IP experiments.
(J) His-importin α3 was purified from *E. coli* BL21. His-importin α3 was incubated with beads binding GST-Sp1 (aa 600–780) with or without O-GlcNAcylation.
See also Table S1.

CellPress

AUTHOR CONTRIBUTIONS

W.T., P.J., W. Zhang, Z.H., S.L., L.C., C.P., Z.L., and A.S. performed the experiments and analyzed the data. Y.X., Q.S., W.Zhu, and F.H. contributed critical reagents and to the experimental design. H.P., F.H., W.Q., and W.T. designed the study, analyzed the data, and wrote the manuscript. All authors discussed the experiments and revised the manuscript.

DECLARATION OF INTERESTS

The authors declare no competing interests.

Received: August 14, 2020
Revised: December 21, 2020
Accepted: February 3, 2021
Published: March 2, 2021

REFERENCES

Altman, B.J., Stine, Z.E., and Dang, C.V. (2016). From Krebs to clinic: glutamine metabolism to cancer therapy. Nat. Rev. Cancer *16*, 749.

Baenke, F., Peck, B., Miess, H., and Schulze, A. (2013). Hooked on fat: the role of lipid synthesis in cancer metabolism and tumour development. Dis. Model. Mech. *6*, 1353–1363.

Bar-Peled, L., and Sabatini, D.M. (2014). Regulation of mTORC1 by amino acids. Trends Cell Biol. *24*, 400–406.

Çağatay, T., and Chook, Y.M. (2018). Karyopherins in cancer. Curr. Opin. Cell Biol. *52*, 30–42.

Cho, S., Hoang, A., Sinha, R., Zhong, X.Y., Fu, X.D., Krainer, A.R., and Ghosh, G. (2011). Interaction between the RNA binding domains of Ser-Arg splicing factor 1 and U1-70K snRNP protein determines early spliceosome assembly. Proc. Natl. Acad. Sci. USA *108*, 8233–8238.

Chung, S.S., Kim, J.H., Park, H.S., Choi, H.H., Lee, K.W., Cho, Y.M., Lee, H.K., and Park, K.S. (2008). Activation of PPARgamma negatively regulates O-GlcNAcylation of Sp1. Biochem. Biophys. Res. Commun. *372*, 713–718.

Currie, E., Schulze, A., Zechner, R., Walther, T.C., and Farese, R.V., Jr. (2013). Cellular fatty acid metabolism and cancer. Cell Metab. *18*, 153–161.

Damiano, F., Alemanno, S., Gnoni, G.V., and Siculella, L. (2010). Translational control of the sterol-regulatory transcription factor SREBP-1 mRNA in response to serum starvation or ER stress is mediated by an internal ribosome entry site. Biochem. J. *429*, 603–612.

de Queiroz, R.M., Carvalho, E., and Dias, W.B. (2014). O-GlcNAcylation: The Sweet Side of the Cancer. Front. Oncol. *4*, 132.

DeBerardinis, R.J., Lum, J.J., Hatzivassiliou, G., and Thompson, C.B. (2008). The biology of cancer: metabolic reprogramming fuels cell growth and proliferation. Cell Metab. *7*, 11–20.

Dias, W.B., and Hart, G.W. (2007). O-GlcNAc modification in diabetes and Alzheimer's disease. Mol. Biosyst. *3*, 766–772.

Dibble, C.C., and Manning, B.D. (2013). Signal integration by mTORC1 coordinates nutrient input with biosynthetic output. Nat. Cell Biol. *15*, 555–564.

Fagerlund, R., Kinnunen, L., Köhler, M., Julkunen, I., and Melén, K. (2005). NF-kappaB is transported into the nucleus by importin alpha3 and importin alpha4. J. Biol. Chem. *280*, 15942–15951.

Gabriel, S.S., and Kallies, A. (2016). Glucose- and glutamine-fueled stabilization of C-Myc is required for T-cell proliferation and malignant transformation. Cell Death Discov. *2*, 16047.

Goldfarb, D.S., Corbett, A.H., Mason, D.A., Harreman, M.T., and Adam, S.A. (2004). Importin alpha: a multipurpose nuclear-transport receptor. Trends Cell Biol. *14*, 505–514.

Hanover, J.A., Krause, M.W., and Love, D.C. (2010). The hexosamine signaling pathway: O-GlcNAc cycling in feast or famine. Biochim. Biophys. Acta *1800*, 80–95.

Hanover, J.A., Krause, M.W., and Love, D.C. (2012). Bittersweet memories: linking metabolism to epigenetics through O-GlcNAcylation. Nat. Rev. Mol. Cell Biol. *13*, 312–321.

Hardivillé, S., and Hart, G.W. (2014). Nutrient regulation of signaling, transcription, and cell physiology by O-GlcNAcylation. Cell Metab. *20*, 208–213.

Hart, G.W., Housley, M.P., and Slawson, C. (2007). Cycling of O-linked beta-N-acetylglucosamine on nucleocytoplasmic proteins. Nature *446*, 1017–1022.

Hart, G.W., Slawson, C., Ramirez-Correa, G., and Lagerlof, O. (2011). Cross talk between O-GlcNAcylation and phosphorylation: roles in signaling, transcription, and chronic disease. Annu. Rev. Biochem. *80*, 825–858.

Hay, N. (2016). Reprogramming glucose metabolism in cancer: can it be exploited for cancer therapy? Nat. Rev. Cancer *16*, 635–649.

Horton, J.D., Goldstein, J.L., and Brown, M.S. (2002). SREBPs: activators of the complete program of cholesterol and fatty acid synthesis in the liver. J. Clin. Invest. *109*, 1125–1131.

Huang, K.Y., Su, M.G., Kao, H.J., Hsieh, Y.C., Jhong, J.H., Cheng, K.H., Huang, H.D., and Lee, T.Y. (2016). dbPTM 2016: 10-year anniversary of a resource for post-translational modification of proteins. Nucleic Acids Res. *44* (D1), D435–D446.

Ito, T., Azumano, M., Uwatoko, C., Itoh, K., and Kuwahara, J. (2009). Role of zinc finger structure in nuclear localization of transcription factor Sp1. Biochem. Biophys. Res. Commun. *380*, 28–32.

Ito, T., Kitamura, H., Uwatoko, C., Azumano, M., Itoh, K., and Kuwahara, J. (2010). Interaction of Sp1 zinc finger with transport factor in the nuclear localization of transcription factor Sp1. Biochem. Biophys. Res. Commun. *403*, 161–166.

Jang, S.W., Yang, S.J., Ehlén, A., Dong, S., Khoury, H., Chen, J., Persson, J.L., and Ye, K. (2008). Serine/arginine protein-specific kinase 2 promotes leukemia cell proliferation by phosphorylating acinus and regulating cyclin A1. Cancer Res. *68*, 4559–4570.

Jang, S.W., Liu, X., Fu, H., Rees, H., Yepes, M., Levey, A., and Ye, K. (2009). Interaction of Akt-phosphorylated SRPK2 with 14-3-3 mediates cell cycle and cell death in neurons. J. Biol. Chem. *284*, 24512–24525.

Kamphorst, J.J., Cross, J.R., Fan, J., de Stanchina, E., Mathew, R., White, E.P., Thompson, C.B., and Rabinowitz, J.D. (2013). Hypoxic and Ras-transformed cells support growth by scavenging unsaturated fatty acids from lysophospholipids. Proc. Natl. Acad. Sci. USA *110*, 8882–8887.

Kelley, J.B., Talley, A.M., Spencer, A., Gioeli, D., and Paschal, B.M. (2010). Karyopherin alpha7 (KPNA7), a divergent member of the importin alpha family of nuclear import receptors. BMC Cell Biol. *11*, 63.

Kohtz, J.D., Jamison, S.F., Will, C.L., Zuo, P., Lührmann, R., Garcia-Blanco, M.A., and Manley, J.L. (1994). Protein-protein interactions and 5′-splice-site recognition in mammalian mRNA precursors. Nature *368*, 119–124.

Kommaddi, R.P., Dickson, K.M., and Barker, P.A. (2011). Stress-induced expression of the p75 neurotrophin receptor is regulated by O-GlcNAcylation of the Sp1 transcription factor. J. Neurochem. *116*, 396–405.

Kreppel, L.K., and Hart, G.W. (1999). Regulation of a cytosolic and nuclear O-GlcNAc transferase. Role of the tetratricopeptide repeats. J. Biol. Chem. *274*, 32015–32022.

Krześlak, A., Forma, E., Bernaciak, M., Romanowicz, H., and Bryś, M. (2012). Gene expression of O-GlcNAc cycling enzymes in human breast cancers. Clin. Exp. Med. *12*, 61–65.

Kuwahara, J., Watanabe, Y., Kayasuga, T., and Itoh, K. (2000). Zn finger and nuclear localization of transcription factor Sp1. Nucleic Acids Symp. Ser. *44*, 265–266.

Lee, G., Zheng, Y., Cho, S., Jang, C., England, C., Dempsey, J.M., Yu, Y., Liu, X., He, L., Cavaliere, P.M., et al. (2017). Post-transcriptional Regulation of De Novo Lipogenesis by mTORC1-S6K1-SRPK2 Signaling. Cell *171*, 1545–1558.e18.

Li, Y., Xu, S., Mihaylova, M.M., Zheng, B., Hou, X., Jiang, B., Park, O., Luo, Z., Lefai, E., Shyy, J.Y., et al. (2011). AMPK phosphorylates and inhibits SREBP activity to attenuate hepatic steatosis and atherosclerosis in diet-induced insulin-resistant mice. Cell Metab. *13*, 376–388.

Li, J., Summerlin, M., Nitiss, K.C., Nitiss, J.L., and Hanakahi, L.A. (2017). TDP1 is required for efficient non-homologous end joining in human cells. DNA Repair (Amst.) *60*, 40–49.

Macara, I.G. (2001). Transport into and out of the nucleus. Microbiol. Mol. Biol. Rev. *65*, 570–594.

Marshall, S., Bacote, V., and Traxinger, R.R. (1991). Discovery of a metabolic pathway mediating glucose-induced desensitization of the glucose transport system. Role of hexosamine biosynthesis in the induction of insulin resistance. J. Biol. Chem. *266*, 4706–4712.

Mathew, R., Hartmuth, K., Möhlmann, S., Urlaub, H., Ficner, R., and Lührmann, R. (2008). Phosphorylation of human PRP28 by SRPK2 is required for integration of the U4/U6-U5 tri-snRNP into the spliceosome. Nat. Struct. Mol. Biol. *15*, 435–443.

Menendez, J.A., and Lupu, R. (2007). Fatty acid synthase and the lipogenic phenotype in cancer pathogenesis. Nat. Rev. Cancer *7*, 763–777.

Miyamoto, Y., Yamada, K., and Yoneda, Y. (2016). Importin α: a key molecule in nuclear transport and non-transport functions. J. Biochem. *160*, 69–75.

Mossmann, D., Park, S., and Hall, M.N. (2018). mTOR signalling and cellular metabolism are mutual determinants in cancer. Nat. Rev. Cancer *18*, 744–757.

Nardozzi, J.D., Lott, K., and Cingolani, G. (2010). Phosphorylation meets nuclear import: a review. Cell Commun. Signal. *8*, 32.

Pavlova, N.N., and Thompson, C.B. (2016). The Emerging Hallmarks of Cancer Metabolism. Cell Metab. *23*, 27–47.

Peng, C., Zhu, Y., Zhang, W., Liao, Q., Chen, Y., Zhao, X., Guo, Q., Shen, P., Zhen, B., Qian, X., et al. (2017). Regulation of the Hippo-YAP Pathway by Glucose Sensor O-GlcNAcylation. Mol. Cell *68*, 591–604.e5.

Pinho, S.S., and Reis, C.A. (2015). Glycosylation in cancer: mechanisms and clinical implications. Nat. Rev. Cancer *15*, 540–555.

Reily, C., Stewart, T.J., Renfrow, M.B., and Novak, J. (2019). Glycosylation in health and disease. Nat. Rev. Nephrol. *15*, 346–366.

Sanjana, Neville, E, Shalem, Ophir, and Zhang, Feng (2014). Improved vectors and genome-wide libraries for CRISPR screening. Nat Methods *11* (8), 783–784, https://doi.org/10.1038/nmeth.3047.

Shalem, O., Sanjana, N.E., Hartenian, E., Shi, X., Scott, D.A., Mikkelson, T., Heckl, D., Ebert, B.L., Root, D.E., Doench, J.G., and Zhang, F. (2014). Genome-scale CRISPR-Cas9 knockout screening in human cells. Science *343*, 84–87.

Shen, D.L., Gloster, T.M., Yuzwa, S.A., and Vocadlo, D.J. (2012). Insights into O-linked N-acetylglucosamine ([0-9]O-GlcNAc) processing and dynamics through kinetic analysis of O-GlcNAc transferase and O-GlcNAcase activity on protein substrates. J. Biol. Chem. *287*, 15395–15408.

Shimano, H., and Sato, R. (2017). SREBP-regulated lipid metabolism: convergent physiology - divergent pathophysiology. Nat. Rev. Endocrinol. *13*, 710–730.

Slawson, C., and Hart, G.W. (2011). O-GlcNAc signalling: implications for cancer cell biology. Nat. Rev. Cancer *11*, 678–684.

Stewart, M. (2007). Molecular mechanism of the nuclear protein import cycle. Nat. Rev. Mol. Cell Biol. *8*, 195–208.

Tani, H., and Akimitsu, N. (2012). Genome-wide technology for determining RNA stability in mammalian cells: historical perspective and recent advantages based on modified nucleotide labeling. RNA Biol. *9*, 1233–1238.

Taylor, R.P., Geisler, T.S., Chambers, J.H., and McClain, D.A. (2009). Up-regulation of O-GlcNAc transferase with glucose deprivation in HepG2 cells is mediated by decreased hexosamine pathway flux. J. Biol. Chem. *284*, 3425–3432.

Vander Heiden, M.G., Cantley, L.C., and Thompson, C.B. (2009). Understanding the Warburg effect: the metabolic requirements of cell proliferation. Science *324*, 1029–1033.

Vernia, S., Edwards, Y.J., Han, M.S., Cavanagh-Kyros, J., Barrett, T., Kim, J.K., and Davis, R.J. (2016). An alternative splicing program promotes adipose tissue thermogenesis. eLife *5*, e17672.

Wang, H.Y., Lin, W., Dyck, J.A., Yeakley, J.M., Songyang, Z., Cantley, L.C., and Fu, X.D. (1998). SRPK2: a differentially expressed SR protein-specific kinase involved in mediating the interaction and localization of pre-mRNA splicing factors in mammalian cells. J. Cell Biol. *140*, 737–750.

Wang, J., Torii, M., Liu, H., Hart, G.W., and Hu, Z.Z. (2011). dbOGAP - an integrated bioinformatics resource for protein O-GlcNAcylation. BMC Bioinformatics *12*, 91.

Wang, G., Sheng, W., Shi, X., Li, X., Zhou, J., and Dong, M. (2019). Serine/arginine protein-specific kinase 2 promotes the development and progression of pancreatic cancer by downregulating Numb and p53. FEBS J. *286*, 1668–1682.

Wu, S., and Näär, A.M. (2019). SREBP1-dependent de novo fatty acid synthesis gene expression is elevated in malignant melanoma and represents a cellular survival trait. Sci. Rep. *9*, 10369.

Yang, X., and Qian, K. (2017). Protein O-GlcNAcylation: emerging mechanisms and functions. Nat. Rev. Mol. Cell Biol. *18*, 452–465.

Yang, X., Ongusaha, P.P., Miles, P.D., Havstad, J.C., Zhang, F., So, W.V., Kudlow, J.E., Michell, R.H., Olefsky, J.M., Field, S.J., and Evans, R.M. (2008). Phosphoinositide signalling links O-GlcNAc transferase to insulin resistance. Nature *451*, 964–969.

STAR★METHODS

KEY RESOURCES TABLE

REAGENT or RESOURCE	SOURCE	IDENTIFIER
Antibodies		
Rabbit polyclonal Anti-pSRPK2(S494)	Millipore	Cat# 07-1817; RRID:AB_11205747
Rabbit polyclonal Anti-pSRPK2(S497)	Millipore	Cat# ABS192; RRID:AB_2888677
Mouse monoclonal Anti-SRPK2	BD Bioscience	Cat# BD611118; RRID:AB_398429
Rabbit polyclonal Anti-ACLY	Cell Signaling Technology	Cat# 4332; RRID:AB_2223744
Rabbit monoclonal Anti-FDFT1	Abcam	Cat# ab109723; RRID:AB_10859772
Rabbit monoclonal Anti-S6K1	Cell Signaling Technology	Cat# 2708; RRID:AB_390722
Rabbit monoclonal Anti-pS6K1(T389)	Cell Signaling Technology	Cat# 9234; RRID:AB_2269803
Rabbit monoclonal Anti-pSR proteins	Invitrogen	Cat# 33-9400; RRID:AB_87195
Mouse monoclonal Anti-actin	Proteintech	Cat# 60008-1; RRID:AB_2289225
Rabbit polyclonal Anti-AMPK	Cell Signaling Technology	Cat# 2532; RRID:AB_330331
Mouse monoclonal Anti-HA	BioLegend	Cat# MMS-101P, Clone 16B12; RRID:AB_2314672
Rabbit monoclonal Anti-HA	Cell Signaling Technology	Cat# C29F4; RRID: AB_1549585
Rabbit monoclonal Anti-OGT	Cell Signaling Technology	Cat# 24083; RRID:AB_2716710
Mouse monoclonal Anti-O-linked N-Acetylglucosamine antibody [RL2]	Abcam	Cat# ab2739; RRID:AB_303264
Rabbit monoclonal Anti-GFPT1	Cell Signaling Technology	Cat# 5322; RRID:AB_10699031
Bacterial and virus strains		
E.coil BL21	New England Biolabs	Cat#C2527
Chemicals, peptides, and recombinant proteins		
Rapamycin	Sigma-Aldrich	Cat# R8781
PUGNAc	Sigma-Aldrich	Cat#7229
Benzyl 2-acetamido-2-deoxy-α-D-galactopyranoside	Sigma-Aldrich	Cat#4894
U-13C-glucose	Cambridge Isotope Laboratories	Cat#4894
Uridine 5′-diphospho-N-acetylglucosamine sodium salt	Sigma-Aldrich	Cat#4375
Puromycin dihydrochloride	Sigma-Aldrich	Cat#9620
G418 Antibiotic Solution	VWR	Cat#97064-358
Critical commercial assays		
BCA protein assay kit	TIANGEN	Cat#PA115
Fast Quant RT Kit BCA protein assay kit	TIANGEN	Cat#KR106
Cell Counting Kit 8	Dojindo	Cat#CK04-11
SsoAdvancedTM Universal SYBR® Green Supermix	BioRad	Cat#1725271
Deposited data		
RNA-seq raw data	This paper	GEO: GSE147725
Original data have been deposited to the Mendeley data	This paper	https://doi.org/10.17632/ww6swsfrp6.1
Experimental models: cell lines		
HEK293T	ATCC	CRL11268
MCF7	ATCC	HTB-22
AMPK−/− MEF cells	Dr. Liewei Wang	N/A
Experimental models: organisms/strains		
Female nude mice	Jackson Lab	Cat#002019

(*Continued on next page*)

Continued

REAGENT or RESOURCE	SOURCE	IDENTIFIER
Oligonucleotides		
si-Cont: UUCUCCGAACGUGUCACGU	This paper	N/A
si-human-OGT-1: GAUUAAGCCUGUUGAAGUC	Peng et al., 2017	N/A
si-human-OGT-2: GCUUGCAAUUCAUCACUUU	Peng et al., 2017	N/A
si-human-GFPT1-1: GCCAGUACAAAGGCUUAUA	This paper	N/A
si-human-GFPT1-2: GGAGAGAGGAGCUUUAACU	This paper	N/A
shRNA-human-SRPK2: CCGGGCACCCTGTAAATGTT ACTTTCTCGAGAAAGTAACATTTACAGGGTGCTTTTT	This paper	N/A
si-mouse-siGFPT1-1	Sigma Aldrich	SASI_Mm01_00170346
si-mouse-siGFPT1-2	Sigma Aldrich	SASI_Mm01_00170347
si-human-SRPK2: GCACCCUGUAAAUGUUACU	This paper	N/A
si-human-importin α5-1: GCCUUUGAUCUUAUUGAGC	This paper	N/A
si-human-importin α5-2: GCAGUUAUUCAAGCGGAGA	This paper	N/A
si-human-importin α1-1: UCAUGUAGCUGAGACAUAA	This paper	N/A
si-human-importin α1-2: GCUGGUUUGAUUCCGAAAU	This paper	N/A
si-human-importin α4-1: UUGUCCUCCACAAACAUAU	This paper	N/A
si-human-importin α4-2: GCUGUAAUAGAUGCUGGAU	This paper	N/A
si-human-importin α3: GCCCUCUCUUACCUUACUG	This paper	N/A
si-human-importin α6-1: CUAUGCUUGAAAGUCCUAU	This paper	N/A
si-human-importin α6-2: CAGUUGUUCAAACGCAGAA	This paper	N/A
si-human-importin α7-1: CGGAGAAAUGUGGAGCUGA	This paper	N/A
si-human-importin α7-2: GCCUGGGCUCUAACGAAUA	This paper	N/A
si-human-importin α8-1: UCAGAUCCAGUCCUAUGUU	This paper	N/A
si-human-importin α8-2: GCUGCAUGAGAACCGUCAA	This paper	N/A
si-human-importin β-1: CGGAGAUCGAAGACUAACA	This paper	N/A
si-human-importin β-2: CCAGUGUAGUUGUUCGAGA	This paper	N/A
Primers for qPCR analysis, see Table S2	This paper	N/A
Recombinant DNA		
Myc-OGT	Dr. X. Yu	N/A
pET28a-His-hOGT	Dr. Shao Feng	N/A
pGEX-4T-2-OGA	Dr. Shao Feng	N/A
pGEX-4T-2-SRPK2 WT, 4A	This paper	N/A
pGEX-4T-2-SRPK2 WT (aa1-540)	This paper	N/A
pGEX-4T-2-SRPK2 WT, S497A, S497D (aa454-521)	This paper	N/A
HA-SRPK2 WT	Lee et al., 2017	N/A
HA-SRPK2 T237A, S490A, S494A, T498A, 4A, 3A, ΔNLS1, ΔNLS2, 494A/497A, K110M	This paper	N/A
pIRES-Flag-importin α3, α5, α6, beta, S6K1	This paper	N/A
pEBB-HA-RELA WT	Addgene	Item#74892
HA-RELA T305A	This paper	N/A
pGEX-4T-2-RELA WT, T305A (aa200-350)	This paper	N/A
pCMV-HA-Sp1 WT, 5A	This paper	N/A
pGEX-4T-2 Sp1 WT, 5A (aa600-780)	This paper	N/A
pET28a-His-importin α3	This paper	N/A
pBS Sp1 WT	Addgene	Item#12096
pCMVTNT-T7-KPNA1, KPNA2, KPNA3, KPNA4, KPNA5, KPNA6, KPNA7	Addgene	Item#26677-26683

(*Continued on next page*)

Continued

REAGENT or RESOURCE	SOURCE	IDENTIFIER
lentiCRISPRv2 vector	Sanjana et al., 2014	N/A
psPAX2, pMD2.G	Addgene	Item#12260, 12259
Software and algorithms		
GraphPad Prism 6.0	GraphPad software	https://www.graphpad.com

RESOURCE AVAILABILITY

Lead contact

Further information and requests for resources and reagents should be directed to and will be fulfilled by the Lead Contact, Huadong Pei (huadongpei@gwu.edu).

Materials availability

Materials generated in this study are available on the request to the lead contact.

Data and code availability

The accession number for the RNA-seq data reported in this paper is GEO: GSE147725.

Original data have been deposited to Mendeley data: https://doi.org/10.17632/ww6swsfrp6.1

EXPERIMENTAL MODEL AND SUBJECT DETAILS

Cell lines

MCF7(ATCC®HTB-22), HEK293T(ATCC®CRL11268), and AMPK−/− MEF cells were cultured in Dulbecco's Modified Eagle Medium (DMEM) supplemented with 10% fetal bovine serum, 100 U/ml penicillin, and 100 μg/ml streptomycin, and incubated at 37°C with 5% CO_2.

Mice

Procedures in mice were performed in accordance with the guidelines of the Institutional Animal Care and Use Committee (IACUC) of George Washington University. Mice were housed in a temperature-controlled environment with a 12-hour light/dark cycle, and enjoyed the food and fresh water *ad libitum*.

Microbe strains

BL21 *Escherichia coli* (*E. coli*) were grown at room temperature (22-25°C) in 1 × Luria Bertani Broth (Sigma, L3022) for protein purification.

METHOD DETAILS

Antibodies and other reagents

Anti-GFPT1, anti-AMPK, anti-OGT, anti-ACLY, anti-S6K, anti-pS6K1, and anti-His antibodies were purchased from Cell Signaling Technology. Anti-FDFT1 and anti-O-linked N-Acetylglucosamine [RL2] antibodies were obtained from Abcam. Anti-SRPK2 antibodies were from BD Biosciences. Anti-FLAG antibodies, anti-SRPK2 pS494 antibodies, anti-pSR antibodies, and anti-HA antibodies were from Sigma-Aldrich, Millipore, Invitrogen, and BioLegend, respectively. Reagents were purchased from following sources: PUGNAc, rapamycin, and BADGP from Sigma-Aldrich; and U-^{13}C-glucose from Cambridge Isotope Laboratories.

mRNA expression analyses

Total RNA was extracted using RNeasy Mini Kit (omega® BIO-TEK). CDNA was prepared using FastQuant RT Kit (TIANGEN), and gene expression was analyzed by real-time PCR (qPCR) using SsoAdvanced™ Universal SYBR® Green Supermix (BioRad) with a Bio-Rad CFX96 instrument. All gene expression levels were normalized to those of the housekeeping genes, such as actin or PPIB. To examine mRNA stability, gene transcription was blocked by actinomycin D (5 μg/ml) treatment for 0, 3, and 6 hr. Reverse transcription was performed using the same volume of RNA for all time points and mRNA levels were measured by qPCR.

Cell viability and colony formation assays

Cell Counting Kit 8 was used to detect cell viability following the manufacturer's instructions. Colony formation assays were performed as previously described (Peng et al., 2017).

Xenograft tumor growth assays

Mouse procedures were performed in accordance with the Guideline of the Institutional Animal Care and Use Committee (IACUC) of George Washington University, Washington DC. Female nude mice (6-8 weeks old) were purchase from the Jackson Laboratory (Bar Harbor, ME). 2×10^6 MCF7 cells were injected subcutaneously into the posterior flank regions of each nude mouse. Tumor width and length were measured using a digital caliper every three days. Tumor volume was calculated using the following formula: $volume = (length \times (width)^2 \div 2)$.

siRNA and shRNA

All small interfering RNA (siRNA) oligonucleotides were purchased from Sigma Aldrich. Cells were transfected with the indicated siRNAs twice at 24 hours intervals using lipofectamine RNAiMAX (Invitrogen). For the rescue experiments in this study, shRNA targeting 3′UTR of SRPK2 (CCGGGCACCCTGTAAATGTTACTTTCTCGAGAAAGTAACATTTACAGGGTGCTTTTT) was used unless otherwise stated.

CRISPR/Cas9 knockout

Guide RNA sequences targeting human SRPK2 (GCATTATACGGAGACAGCCT, GGATCCGCGGAATGCAGATA, and GACGCGT CAGTACCGCTCCA) were synthesized and cloned into a lentiCRISPRv2 vector as previously described (Shalem et al., 2014). MCF7 cells and HEK293T cells were infected with viral supernatants and selected with puromycin at the indicated concentrations (outlined below). To obtain the single cell clone, infected cells were diluted and seeded into 96-well plates. The knockout efficiency of SRPK2 was confirmed by immunoblotting.

Generation of stable cell lines

Lentiviruses were produced as previously described (http://www.addgene.org/protocols/plko/#E). Transfections were carried out using the polyethylenimine (PEI) method at a ratio of PEI:cDNA (pMD2.G: psPAX2: viral vectors) = 10:1. The virus-containing medium was harvested 48 and 72 hours after transfection and subsequently filtered with a 0.45 μm filter (Millipore). The virus-containing medium was concentrated with PEG8000 reagents (4:1, v/v). The indicated cells were infected with the concentrated virus with 8 μg/ml polybrene, and selected using different doses of puromycin: MCF7 or 293T cells, 2 μg/ml.

Cell lysis, immunoprecipitation, and immunoblotting

Cells were collected and lysed on ice using NETN buffer (100 mM NaCl, 10 mM Tris-HCl [pH 8.0], 0.5% NP-40 and 1 mM EDTA) supplemented with 1 × protease inhibitors (Roche). After sonication, cell lysates were centrifuged at 12,000 rpm at 4°C for 10 min. The protein solution was quantified using a BCA protein assay kit (TIANGEN). 5-15 μg of protein were analyzed by immunoblotting with indicated antibodies. The immunoblotting images were captured with an Odyssey® Fc Imaging System (LI-COR).

For immunoprecipitation of endogenous SRPK2 or OGT, cells were lysed with NETN buffer and incubated with anti-SRPK2 or OGT primary antibodies at 4°C for 4 hours, followed by incubation with the 50% slurry of protein A/G Sepharose beads (GE Healthcare Life Sciences) presaturated with NETN buffer for an additional 2 hours. Beads were washed three times with NETN lysis buffer and samples were subjected to immunoblotting with the indicated antibodies.

To immunoprecipitate endogenous SRPK2 or WT/mutant HA-SRPK2 for O-GlcNAcylation examination, cells were lysed with NETN buffer supplemented with 100 μM PUGNAc (OGA inhibitor). Cell lysates were incubated with either protein A/G Sepharose beads (Santa Cruz Biotechnology) or anti-HA beads (Sigma Aldrich) at 4°C for 4 hours. Beads were washed three times with NETN lysis buffer. Samples were separated by SDS-PAGE and subjected to immunoblotting with the indicated antibodies.

Protein purification

For GST-tagged protein purification, *E. coli* BL21 cells were transformed with the target plasmids. Cell cultures were grown at 37°C with shaking until the cell density reached 600 nm (OD600) of 0.6. Expression of recombinant genes was induced with 0.2 mM of isopropyl β-d-1-thiogalactopyranoside (IPTG) overnight. GST fusion protein was purified using glutathione-Sepharose 4B beads as previously described.

O-GlcNAcylated SRPK2 purification was performed as previously described (Shen et al., 2012). pGEX-4T-SRPK2 and pET28a-hOGT (aa323-1041) were co-transformed into *E. coli* BL21 and the signal colony was selected on a Luria Bertani agar plate containing 100 μg/ml ampicillin and 50 μg/ml kanamycin for next expanding culture. The subsequent steps were the same as the GST fusion protein purification procedure described above.

For His-tagged protein purification, *E. coli* BL21 cells were transformed with pET28a-hOGT (aa323-1041) plasmid. The bacterial culture was grown until it reached at the OD600 value of 0.6-0.8. Then 0.2 mM of IPTG was added overnight to induce protein expression. Bacterial cells were harvested, re-suspended in ice-cold lysis buffer (500 mM NaCl, 5 mM imidazole, and 20 mM Tris-pH 7.9) (Li et al., 2017) containing 0.1% Triton X-100 and a protease inhibitor (Rocher) and lysed with a sonicator. His-tagged proteins were purified with Ni-NTA (GE Healthcare) as previously described.

S6K1 kinase assays in recombinant SRPK2

FLAG-S6K1 protein was overexpressed and purified from HEK293T cells. For S6K1 *in vitro* kinase assays, 1 μg of bacterially-expressed GST-SRPK2 or O-GlcNAcylated GST-SRPK2 were incubated with purified FLAG-S6K1 in a 50 μl reaction volume containing

25 mM Tris/HCl pH 7.5, 10 mM $MgCl_2$, 5 mM β-glycerophosphate, 2 mM DTT, and 100 μM ATP at 30°C for 1 hour. Samples were separated by SDS-PAGE and subjected to immunoblotting with the indicated antibodies.

In vitro O-GlcNAcylation assays

Because GST-tagged full-length human OGT had limited activity *in vitro*, we used the enzyme domain of human OGT (Cys323-Glu1041) for *in vitro* O-GlcNAcylation assays. Recombinant His-OGT protein (aa323-1041) (1 μg) was incubated with 2 μg of recombinant GST-SRPK2 (aa454-521) or its mutant in 60 μL reaction volume (50 mM Tris-HCl, 12.5 mM $MgCl_2$, 2 mM UDP-GlcNAc 1 mM DTT, pH 7.5) at 37°C for 4 hours. Samples were separated by SDS-PAGE and subjected to immunoblotting with the indicated antibodies.

OGA treatment assays

The assay has been described previously. Briefly, O-GlcNAcylated SRPK2 protein (by *in vitro* O-GlcNAcylation assay) was incubated with 5 μg Clostridium perfringens OGA (aa31-624) at 37°C for 4 hours in a volume of 60 μl. Then samples were boiled with SDS-loading buffer for immunoblotting analysis.

GST pull-down assays

GST-SRPK2 fusion protein was purified from *E. coli* BL21 cells and immobilized on glutathione Sepharose 4B columns (GE Healthcare). HEK293T cells transfected with the indicated plasmids were lysed in NETN buffer with protease inhibitor cocktail (Sigma-Aldrich, USA) and incubated with Sepharose beads immobilized with the indicated GST-tagged proteins at 4 °C overnight. After washing three times with NETN buffer, beads were boiled in 60 μl 2 × SDS loading buffer and subjected to immunoblotting with the indicated antibodies.

Immunofluorescence staining

The assay has been described previously. Briefly, cells were seeded on glass coverslips in 6-well plates. After the indicated treatment, cells were fixed with 3% methanol-free formaldehyde at room temperature for 15 min and rinsed once with PBS. Then, the cells were incubated with 0.5% Triton X-100 for 5 min at room temperature. Next, the cells were incubated with blocking buffer (5% goat serum in PBS) for 1 hour at room temperature. After blocking, the fixed cells were incubated with primary antibody overnight at 4 °C (SRPK2, 1:100 dilution in the blocking buffer). Cells were then washed three times with PBS, incubated with secondary antibodies conjugated with FITC or with TRITC (1:200 dilution in the blocking buffer) at room temperature for 1 hour, and rinsed three times with PBS. Cells were incubated with 0.5 μg/ml DAPI in PBS for 2 min, rinsed once with PBS, and mounted onto the glass slides with mounting medium. Images were taken by the Nikon DS-Ri2 microscope or the Nikon A1RSi confocal microscope.

Human whole transcriptome RNA-seq

Quality of total RNA samples was assessed with Agilent 2100 Bioanalyzer system and library preparation was performed with NEBNext® Ultra II RNA library prep Kit for Illumina® with Poly-A selection according to manufacturer's instructions. Sample sequencing was performed on an Illumina 2 × 150 using mRNA derived from three biological replicates. The reads obtained by RNA-seq were aligned with STAR (2.7.0) against reference genome *Homo sapiens* (GRCh38). HT-Seq (0.11.2) was used to count the gene expression. Subsequently, differential expression was assessed using DEseq2 (1.22.2). The differential alternative splicing analysis is done using rMATs. RNA-seq data have been deposited in the Gene Expression Omnibus (GEO: GSE147725).

Surface plasmon resonance (SPR) analysis

The interaction between the GST-tagged importinα3 and the SRPK2 O-GlcNAc-NLS (or NLS) was monitored by SPR using a Biacore T200 (GE Healthcare) carried out at 25°C in single-cycle mode. The CM5 biosensor chip (GE Healthcare) was immobilized with the GST tagged-importin α3 and GST tag (negative control) according to manufacturer's protocol and tested for binding with gradient concentrations of the O-GlcNAc-NLS (HDRS(O-GlcNAc)RT(O-GlcNAc)VSASST(O-GlcNAc)GDLPKAKTR AADLLVNPLDPRNADK-Biotin) and NLS peptides (HDRSRTVSAS STGDLPKAKTRAADLLVNPLDPRNADK-Biotin). The SRPK2 O-GlcNAc-NLS and NLS peptides were dissolved in buffer containing 20 mM HEPES (pH 7.4), 150 mM NaCl, and 0.005% (v/v) Tween 20. Next, various concentrations of O-GlcNAc-NLS and NLS were flowed through the chip and the real-time responses were recorded. The concentrations of O-GlcNAc-NLS and NLS peptides were 0.39, 0.78, 1.56, 3.12, 6.25, 12.5, 25, 50 and 100 nM, when testing interactions with importin α3. After each reaction, the chip was re-generated using pH 1.7 glycine. The equilibrium dissociation constants (KD) for each pair of interaction were calculated using Biacore T200 evaluation software (GE Healthcare). The KD values were calculated using the model of 1:1 (Langmuir) binding mode.

Sample preparation for MS analyses

For fatty acids, cells were cultured in glucose-free DMEM supplemented with 17.5 mM [U-^{13}C]-glucose (Cambridge Isotope Laboratories) with or without 10% FBS for 48 hours. The cells were gently washed with PBS buffer for three times to remove the medium and were lysed for 90 s in lysis buffer containing 0.3 M KOH in 90% methanol. Next, the lysates were hydrolyzed for 1 hour at 80°C to saponify fatty acids. After adding 10% (v/v) formic acid to neutralize samples, the resulting fatty acids and cell debris

were extracted twice with 1 mL of hexane. Finally, the samples were dried under nitrogen and stored in a −80°C freezer before LC-MS analysis.

For UDP-GlcNAc, after the indicated treatment, cells were cultured in normal DMEM with or without 10% FBS for 48 hours. After washing with PBS three times, the cells were mixed with 80% (v/v) methanol (pre-chilled to −80°C) and incubated at −80°C overnight. Next, the cell lysate in methanol was centrifuged at 14,000 g for 20 min at 4°C before transferring the UDP-GlcNAc containing supernatant to a new 1.5 mL tube on dry ice. UDP-GlcNAc samples were concentrated to dryness under nitrogen and stored in a −80°C freezer before LC-MS analysis.

For cholesterol, after the indicated treatment, cells were harvested and weighted after lyophilization. The lyophilized powders were added with 500 μL 50% (v/v) methanol and sonicated for 5 min. And then, the suspensions were saponified by adding 500 μL 45% (m/v) KOH and incubated for 2 hours at 60°C. After saponification, the suspensions were cooled down to room temperature. Then 500 μL of dichloromethane (DCM) was added, inducing a two-phase separation. The samples were vortexed for 30 s and centrifuged at 1000 r*cf.* for 5min. The bottom phase (containing primarily DCM) was removed. And an additional aliquot of DCM was added to the top phase, vortexed, centrifuged, and the bottom phased was pooled with the previous organic phases. The mixture was dried with nitrogen gas and then resuspended in 200 μL of 9:1 MeOH/H2O (v/v) for LC-MS/MS analysis.

LC-MS analyses of fatty acids, UDP-GlcNAc and cholesterol

Fatty acids and UDP-GlcNAc were analyzed using an Acquity I-Class ultrahigh performance liquid chromatography system equipped with a Waters Vion-IMS-QToF mass spectrometer. Chromatographic separation of fatty acids was performed using an Acquity UPLC-BEH C18 column (100 mm × 2.1 mm i.d., 1.7 μm) with a flow rate of 0.2 mL/min and column temperature of 60°C. Eluent A was 60/40 (v/v) acetonitrile/water with 10 mM ammonium acetate and eluent B was 90/10 (v/v) isopropanol/acetonitrile. Separation was done under the following linear conditions: 0-2.5 min 30% B, 2.5-8 min 50% B, 8-10 min 98% B, 10-15 min 98% B, 15-15.1 min 30% B, and 15.1-18 min 30% B. Chromatographic separation of UDP-GlcNAc was performed using eluent A containing 95/5 (v/v) water/acetonitrile with 10 mM ammonium acetate and eluent B containing 5/95 (v/v) water/acetonitrile. The gradient conditions were set as follows: 0 min 70% B, 0-2 min 40% B, 2-8 min 10% B, 8-9 min 2% B, 9-10 min 2% B, 10-10.1 min 70% B, and 10.1-13 min 70% B.

Fatty acids and UDP-GlcNAc were detected in negative ion mode within a mass range from 50 to 1000 m/z. Lock mass correction was carried out with leucine enkephalin every 2 min. MS conditions were set as follows: capillary voltage 2.5 kV, scan time 0.1 s, low collision energy 6 eV, and collision energy (MSE) starting at 20.00 eV and ending at 30.00 eV for fatty acids and starting at 20.00 eV and ending at 40.00 eV for UDP-GlcNAc. UDP-GlcNAc detection was carried out in the Ion Mobility condition.

Cholesterol was analyzed on a Vion-IMS-QToF Mass Spectrometer equipped with an Acquity I-Class ultrahigh performance liquid chromatography system. The extracts were separated by an Acquity I-Class UPLC (Waters, USA) with an HSS T3-C18 column (2.1 × 100 mm, 1.8 μm) from Waters. 0.1% formic acid was used as the mobile phase A and methanol was used as the mobile phase B. A total flow rate of 0.3 mL/min was set for separation and the gradient was as follows: 0–3 min, 93% B; 3–6 min, 93%–100% B; 6–10 min, 100% B; 10–12 min, 100%–93% B. Metabolites were detected using a Waters Vion-IMS-QToF MS/MS in positive mode within a mass range from 300 to 500 m/z, and other MS conditions was consistent with the fatty acid analysis.

LC-MS/MS analyses for O-GlcNAc identification of SRPK2

SRPK2 purified from HEK293T cells was trypsinized (sequencing grade, Promega, protein: trypsin = 50:1), digested at 37°C for 16 hours, and desalted using C_{18} Zip-Tips (Millipore). LC-MS/MS analyses were carried out using an Easy nLC-1000 system coupled with an Orbitrap Fusion Lumos Tribrid mass spectrometer (Thermo Fisher Scientific). Samples were separated using customized 12 cm length reverse phase columns (150 μm i.d.) packed with Ultimate XB-C_{18} 1.9 μm resin (Welch Materials). A binary solvent system consisting of buffer A (0.1% formic acid in water) and buffer B (0.1% formic acid in acetonitrile) was employed for chromatographic separation with a constant flow rate of 600 nl/min. The gradient was set as follows: 5%–8% B for 8 min, 8%–22% B for 50 min, 22%–32% B for 12 min, 32%–90% B for 1 min, and 90% B for 7 min. The ion source parameters were set as: spray voltage of 2kv, Slens RF level of 30, and ion transfer tube temperature of 300°C. The eluted peptides were analyzed by data-dependent MS2 acquisition (DDA) with a dynamic exclusion duration of 18 s. Higher-energy collision dissociation with a normalized collision energy of 30% was used for peptide fragmentation. The resolution of the MS scan was 120,000, the AGC value was 3e5, and the maximum injection time was 50 ms.

LS-MS data analyses

For quantification of fatty acids and UDP-GlcNAc, MS data were processed using UNIFI software 1.9.3 version (Waters MS Technologies, Manchester, United Kingdom) with natural isotope correction. Deconvolution and peak picking were conducted using 3D peak detection. *De novo* synthesized fatty acids were determined based on the sum of all forms containing four or more labeled carbon atoms (fatty acids containing 2-labeled carbon atoms were made from elongation, not *de novo* synthesis).

For O-GlcNAc identification of SRPK2, tandem mass spectra were searched against the human SRPK2 sequence (UniProtKB: P78362) using Maxquant (version 1.6.10.43). Trypsin was selected as the proteolytic enzyme allowing a maximum of two missed cleavages. Cysteine carbamidomethylation (57.021 Da) was set as the fixed modification. Serine/threonine O-GlcNAcylation (203.079 Da), N-terminal acylation (42.001 Da), and methionine oxidation (15.995 Da) were set as the variable modifications. A false

discovery rate of PSM, proteins, and peptides, was set as less than 1%. Score and delta scores for modified peptides were set to be higher than 40 and 8, respectively. Tandem mass spectra corresponding to the putative O-GlcNAc-modified peptides and sites were verified by manual inspection of their fragmentation patterns.

QUANTIFICATION AND STATISTICAL ANALYSIS

Student's t test and ANOVA were separately used to analyze the data come from two groups and multiple groups. Statistical significance was described by *p* value in the figure legends and methods.